Highly Adsorptive Organic Xerogels for Efficient Removal of Metformin from Aqueous Solutions: Experimental and Theoretical Approach

S. A. Aguilar-Maruri [1,*], D. Perera-Triana [1], Elizabeth Flórez [2], Angélica Forgionny [2], Gabriela Palestino [1], C. F. A. Gómez-Durán [1] and Raúl Ocampo-Pérez [1]

[1] Centro de Investigación y Estudios de Posgrado, Facultad de Ciencias Químicas, Universidad Autónoma de San Luis Potosí, San Luis Potosí 78260, Mexico; a324928@alumnos.uaslp.mx (D.P.-T.); palestinogabriela@uaslp.mx (G.P.); azael.gomez@uaslp.mx (C.F.A.G.-D.); raul.ocampo@uaslp.mx (R.O.-P.)

[2] Grupo de Investigación de Materiales con Impacto (MAT&MPAC), Facultad de Ciencias Básicas, Universidad de Medellín, Medellín 050026, Colombia; mforgionny@udemedellin.edu.co (A.F.)

* Correspondence: a348454@alumnos.uaslp.mx

Abstract: Metformin, widely prescribed to treat type 2 diabetes for its effectiveness and low cost, has raised concerns about its presence in aqueous effluents and its potential environmental and public health impacts. To address this issue, xerogels were synthesized from resorcinol and formaldehyde, with molar ratios ranging from 0.05 to 0.40. These xerogels were thoroughly characterized using FT-IR, SEM, TGA, and TEM analyses. Batch adsorption experiments were performed with standard metformin solutions at concentrations of 50 and 500 mg/L, varying pH, and temperature to determine the adsorption isotherms of the synthesized xerogels. The adsorption data revealed a maximum adsorption capacity of 325 mg/g at pH 11 and 25 °C. Quantum chemical calculations revealed that electrostatic interactions govern metformin adsorption onto xerogels. The xerogels' adsorption capacity was evaluated in competitive systems with $CaCl_2$, NaCl, $MgCl_2$, and synthetic urines. Reuse cycles demonstrated that xerogels could be reused for up to three cycles without any loss in adsorptive efficiency. The adsorption mechanisms of metformin in the adsorption process highlight the strong electrostatic interactions and hydrogen bonds between the adsorbate and the adsorbent material. Xerogels synthesized show promise as efficient adsorbents to remove metformin from aqueous solutions, helping to mitigate its environmental impact.

Keywords: metformin; xerogels; adsorption

1. Introduction

The regulation of discharge concentrations of emerging contaminants in water effluents is currently a global concern. Even at concentrations as low as ppb (μg/L) to ppm (mg/L), these pollutants can degrade environment quality and have a direct impact on human health, leading to deficiencies in ensuring the availability of safe drinking water [1,2]. Furthermore, emerging contaminants like pharmaceuticals, personal care products, pesticides, herbicides, dyes, and industrial chemicals such as hydrocarbons are increasingly being recognized as significant contributors to water pollution [3].

For these reasons, emerging pollutants have received significant attention in recent years due to their anthropogenic origins and the absence of well-established regulations governing their disposal [1,4]. It is estimated that globally, there are approximately 350,000 synthetic compounds for which the disposal and control processes remain uncertain [3]. Among these emerging pollutants, pharmaceutical compounds pose a particularly challenging removal process from water due to their complex nature. These compounds exhibit high solubility in water because of their polar properties, and their ionization degree varies depending on pH levels. In addition, pharmaceutical compounds have a slow

biological and chemical degradation rate, leading to bioaccumulation and the persistence of recalcitrant systems [1–3].

Metformin, the world's second most widely prescribed drug, is a polar compound with ionizable groups, high solubility, and stability in water [5,6]. It serves as an oral antihyperglycemic medication, particularly effective in managing diabetes mellitus in patients who do not require insulin, as it increases the biological effectiveness of available exogenous/endogenic insulin [6–9]. In recent years, metformin has found applications beyond its primary use, including weight loss, antiketogenic activity, and even treatment for patients with COVID-19 [6]. However, there is a concerning issue associated with this drug, which is its potential to induce cancer in prolonged periods of exposure and reduce or damage fertility in both humans and animals [6,9]. In Mexico, concentrations of 0.0103–107 µg/L and 1.29–1.33 µg/L were found in groundwater and hospital wastewater, respectively [6]. In particular, the cationic form of metformin interacts with cell receptors in the liver and peripheral tissues. This interaction produces hypoglycemia by reducing hepatic glucose production and enhancing insulin sensitivity.

The adsorption process is a conventional remediation methodology for emerging contaminant removal from aqueous sources [10]. Several studies have explored various adsorbent materials for removing metformin from aqueous solutions. These materials include hydrocarbons [11], graphene oxides [8]), modified polymeric nanocomposite hydrogels [12], molecularly imprinted polymers [13], and activated carbons [14,15]. However, the adsorption capacities of these current adsorbents are relatively low, ranging from 45 mg/g to 123 mg/g, necessitating either large fixed-bed columns or frequent replacement of exhausted adsorbents. Therefore, it is critical to develop adsorbent materials with higher adsorption capacities.

Xerogels are polymeric matrices with well-defined morphologies [16]. They have many hydroxyl groups on their surface, promoting hydrogen bond formation. Hence, the adsorption mechanism of metformin onto xerogels could occur via hydrogen bonding, where atoms' electronegativity differences facilitate the formation of partial charges on oxygen and hydrogen atoms in the hydroxyl group and the amino group, respectively. These charge disparities enable the formation of hydrogen bonds, with the hydrogen in the hydroxyl group acting as a bridge between the hydroxyl and amino groups, forming weak bonds with the oxygen and nitrogen atoms. These hydrogen bonds are crucial in stabilizing the adsorption process [17].

This work aims to efficiently remove metformin from aqueous solutions using xerogels like adsorbent materials obtained by the resorcinol and formaldehyde (R-F) reaction, with varying molar ratios. These xerogels have not been previously proposed as metformin adsorbents, representing a novel approach to tackling the environmental issue posed by the increasing presence of metformin in wastewater. Therefore, this study will conduct a comprehensive investigation to optimize the adsorption process using xerogels. It will explore metformin dosage, solution temperature, pH, and co-existing ions (salts) concentration. The research also includes an examination of the thermodynamics of the adsorption process, the reuse cycles of the adsorbent material, the effectiveness of the desorption process, and the performance of the xerogels in synthetic urine solutions.

2. Materials and Methods

2.1. Reactants

The synthesis precursors of the xerogels are resorcinol (Purity of 99 wt. %, CAS Number 108-46-3, provided by Productos Químicos Monterrey), formaldehyde (37 wt. % in methanol, CAS Number 50-00-0 provided by Fermont), and NaHCO$_3$ (Purity of 99.5 wt. %, CAS Number 144-55-8 supplied by Karal). The metformin (1,1-Dimethylbiguanide hydrochloride) has a purity grade of 97 wt % (CAS Number 1115-70-4, provided by Sigma Aldrich). The physicochemical properties of metformin are presented in Table 1, emphasizing the crucial role of its water solubility and pKa values in the adsorption process in aqueous solutions. High solubility translates to extensive dispersion in water bodies, which

directly affects the effectiveness of the adsorption process because its high solubility in water will directly impact its affinity for the adsorbent surface. If the adsorbent surface cannot establish strong interactions with metformin, the adsorption process may be inefficient, with equilibrium shifting towards solution phase rather than the adsorbent surface. The pKa values play a crucial role in constructing speciation diagrams and predicting how metformin will ionize in a solution as a function of pH. Understanding metformin's ionization is fundamental across biological, pharmacological, and chemical systems. Figure S1 (see Supplementary Materials) shows the metformin's speciation curve: (a) at pH < 2.8, metformin is predominantly found in its dicationic form; (b) at neutral pH (7.4), metformin primarily adopts its cationic form; and (c) at alkaline pH > 12, metformin mainly exits in its neutral form [1]. The analysis of the conformational characteristics of metformin focuses on its three torsion angles of the main chain, observing that there are two isomers of the monoprotonated form [2]. Although both forms are stabilized by a strong intramolecular hydrogen bond between the imino groups (NH), they are separated by a considerable energetic difference (incremental E = 1.03 kcal mol^{-1}).

Table 1. Physicochemical properties of metformin [3,4].

Property	Value
Name	Metformin Hydrochloride (1,1-Dimethylbiguanide hydrochloride)
CAS number	1115-70-4
Molecular Formula	$C_4H_{11}N_5 \cdot HCl$
Structure	
Molecular weight (g/mol)	165.62
Water solubility (mg/mL at 25 °C)	300
pKa (experimental)	2.8 and 11.5
Vapor pressure (kPa at 20 °C)	<0.000001 kPa
Melting point (°C)	223–226
Boiling point (°C at 760 mmHg)	224.1
Molecular dimensions	
x (Å)	10.83
y (Å)	4.25
z (Å)	1.8
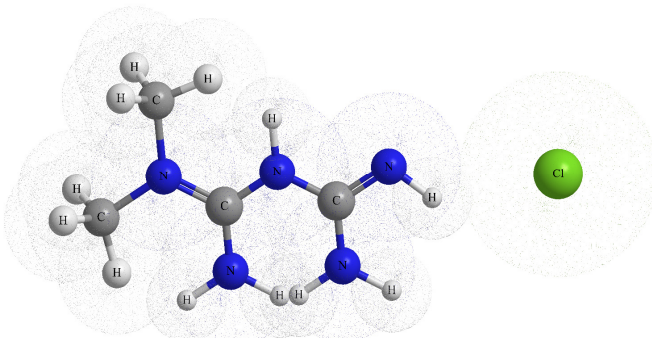
2.2. Xerogel Synthesis

In this work, five xerogel samples were synthesized using molar ratios R:F (Resorcinol–Formaldehyde) of 0.05, 0.15, 0.25, 0.30, and 0.40, keeping constant the F:C (Formaldehyde–NaHCO$_3$) and F:W (Formaldehyde–Water) molar ratios as 2.0 and 0.04, respectively. The xerogels were obtained according to the sequence of the following steps (Figure 1): First, the corresponding mass of water and NaHCO$_3$ is placed in a glass of precipitates at 300 rpm for 10 min. Secondly, the resorcinol was added, and the stirring at 350 rpm continued for

5 min; the specified volume of formaldehyde was incorporated into the solution. Stirring continued at 400 rpm for 45 min at room temperature. The resulting solution is transferred to test tubes, which are hermetically sealed to prevent the evaporation of formaldehyde. The red solutions are placed in a stove heated at 30 °C for 24 h. Subsequently, the temperature is raised to 50 °C for 24 h with the tubes closed. Finally, the tubes are opened and subjected to 80 °C for 120 h. The materials obtained are ground and sieved to obtain an average particle size of 149 μm.
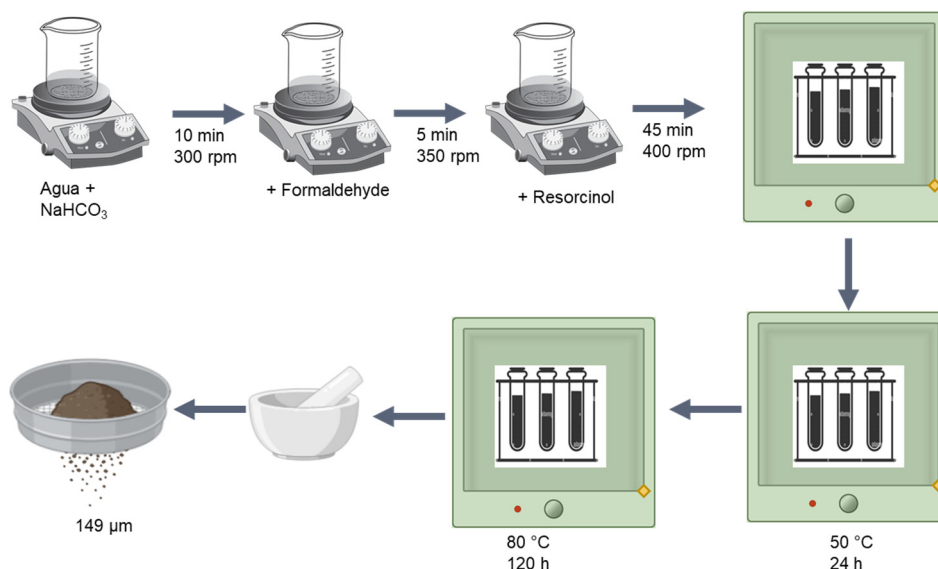
Figure 1. Approach to experimental development for the generation of xerogels.

2.3. Characterization of Xerogels

Physicochemical characterization of the samples was performed using different analysis techniques. The FT-IR spectrometer (Thermo Scientific, model Nicolet iS10, WI, EE) was used to identify functional groups in xerogels and synthesis reagents, equipped with an attenuated total reflection (ATR) fixture with a diamond crystal. A frequency range of 450 to 4000 cm^{-1} was used, with a resolution of 8 cm^{-1}. The surface morphology of xerogels and the mapping of surface elements was observed using SEM (scanning electron microscopy, Helios Nanolab 600), and coupling elemental mapping was performed with EDS (energy-dispersive spectroscopy, Genesis EDS X-ray microanalysis system). The material's crystalline structure was analyzed employing an X-ray diffraction system (PANalytical, X'Pert PRO powder diffraction, λ = 1.54 Å, Xe/methane gas proportional detector). The thermal stability of the xerogels and the processes associated with their decomposition were characterized using a TGA (Thermogravimetric Analyzer, model TA TGA 550) in an Ar atmosphere with a heating rate of 10 °C/min between 29 and 900 °C.

The type and quantification of active sites were determined using the acid-base technique proposed by Boehm [5]. For this purpose, solutions of 0.01 N of NaOH (for total acid sites), and 0.01 N of HCl (for total basic acid sites) were used.

The pH of the point of zero charge (pH_{PZC}) was determined for the xerogels using the acid-base titration procedure proposed by Kuzin and Loskutov [6]. Solutions of 0.1 N of HCl and 0.1 N of NaOH were used, with dilution factors from 5 to 250. A volume of 25 mL of the solutions was added to 0.05 g of xerogel, with constant stirring at 25 °C for seven days, preserving a blank without xerogel. The pH_{final} versus $pH_{initial}$ was plotted, and pH_{PZC} was determined by the point of intersection between the potentiometric titration curves of the solution in the presence and absence of the adsorbent, commonly called the experimental target in adsorption studies.

2.4. Determination of Metformin in Aqueous Solution

The spectrophotometer Shimadzu UV-1900-1 at λ = 232 nm allowed the determination of the concentration of metformin in the prepared aqueous solutions. For an adequate analysis, a calibration curve of 1 to 10 mg/L was used where the absorbance behaves linearly to satisfy the Lambert–Beer law.

2.5. Metformin Adsorption Equilibrium

The experimental data of the adsorption equilibrium were obtained by performing experiments in batch mode. A 50 mL centrifuge tube was used as a batch reactor, where 40 mL of metformin solutions was contacted with 20 mg of adsorbent material at constant pH and temperature. The initial concentration of the solutions was varied from 50 to 500 mg/L. The adsorption equilibrium was obtained at pH 3, 7, and 11. The desired pH was obtained by mixing 0.1 N of NaOH or HCl solutions as required. Throughout the entire time interval, the pH of the solutions was kept constant by adding drops of 0.01 N of NaOH or HCl. Experiments at different temperatures were conducted, placing the batch reactors in an incubator (15 °C) or thermal bath (25 and 45 °C). The experiments were allowed to remain in contact for seven days to reach equilibrium. Subsequently, the adsorbent particles were separated by decantation, and the remaining solution was analyzed to determine the equilibrium concentration of metformin. Finally, from Equation (1), the adsorption capacity was determined.

$$q_e = \frac{V(C_i - C_e)}{m_{ad}} \tag{1}$$

where q_e is the concentration of metformin adsorbed at equilibrium, mg/g; C_i is the initial concentration, mg/L; C_e is the metformin concentration at equilibrium, mg/L; m_{ad} is the mass of the adsorbent, g; and V is the volume of the solution, L. The effect of the presence of salts on the adsorption equilibrium was evaluated by using 0.5, 0.1, and 0.05 M solutions of $CaCl_2$, $MgCl_2$, and NaCl at pH 7 ± 0.05. Finally, to evaluate the applicability of the adsorbents in complex systems, the adsorption equilibrium was evaluated using two synthetic urine solutions. The first one was prepared by adding Na^+ (5.40 g/L), K^+ (0.20 g/L), Mg^{2+} (0.65 g/L), Ca^{2+} (0.50 g/L), Cl^- (9.60 g/L), SO_4^{2-} (1.35 g/L) and urea (17.0 g/L), whereas the second one had the same components but with creatine (2.0 g/L) as an additional component [7].

The adsorption isotherms, having the values of q_e (mg/g, concentration of metformin adsorbed at equilibrium) and C_e (mg/L, metformin concentration at equilibrium), were adjusted to the following mathematical models [8];

Freundlich $$q_e = K_F C_e^{\left(\frac{1}{n_F}\right)} \tag{2}$$

Prausnitz–Radke $$q_e = \frac{aC_e}{1 + bC_e^{\beta}} \tag{3}$$

Langmuir $$q_e = \frac{q_m K_L C_e}{1 + K_L C_e} \tag{4}$$

where K_F is the equilibrium constant of the Freundlich isotherm, $L^{1/n}\ mg^{1-1/n}\ g^{-1}$, n is a constant related to the adsorption intensity; a is the constant of the isotherm of Prausnitz–Radke, L/g, b is the constant of the isotherm of Prausnitz–Radke, L^{β}/g^{β}, β is the constant of the isotherm of Prausnitz–Radke, and q_m is the maximum mass of adsorbed solute on the adsorbent, mg/g, K_L is the constant related to the adsorption equilibrium, L/mg for Langmuir isotherm.

The parameters of these isotherms are evaluated by adjusting the isothermal models with the experimental data using the Levenberg–Marquardt algorithm. The model that

best fits the data is chosen considering the lowest percentage of absolute average deviation, calculated using Equation (5):

$$\% \, Dev = \left(\frac{1}{N} \sum_{i=1}^{N} \left| \frac{q_{e,exp} - q_{e,model}}{q_{e,exp}} \right| \right) 100\% \tag{5}$$

2.6. DFT Calculations

Quantum Chemistry calculations were performed to simulate metformin interaction with xerogel models. First-principles calculations were carried out using the density functional theory framework (DFT). Calculations were conducted using the Gaussian09 software package [9] and the DFT-B3LYP method. The bases 6-311++g(d,p) were used for C, H, O, and N. Geometry optimization calculations and vibrational frequency analysis were performed in the gas phase and considering the solvent effect. This effect was modeled using the integral equation formalism variant of the polarized continuum model (IEFPCM), which contemplates long-range implicit hydration. A model structure was selected to represent xerogels accurately based on experimental findings and the general structure shown in Figure 1. The specific structure used in the DFT simulations is presented in the Supplementary Materials (Figure S2). This model features 3 aromatic rings with high substitution of ether and hydroxyl groups, reflecting the key structural characteristics of xerogels. Moreover, two different xerogel models were simulated to account for pH-dependent behavior: neutral and negatively charged xerogel molecules (Xer and Xer$^-$) considering one or two negative charges.

The initial geometries for xerogel–metformin interactions were determined based on the medium's pH, the material's point of zero charge (pH$_{PZC}$), and metformin's speciation curve. Molecular simulations were conducted at three distinct pH levels: 2, 7, and 11, with xerogel models tailored to each condition: at pH 2, a neutrally charged xerogel model (Xer), at pH 7, both neutral (Xer) and negatively charged (Xer$^-$) xerogel models, and at pH 11, a negatively charged xerogel model (Xer$^-$). Additionally, considering the three pH values mentioned and the speciation curve of metformin related to its protonation–deprotonation states (see Supplementary Materials Figure S1), four different forms of metformin were considered: neutral form (Met), monoprotonated forms (1Met$^+$ and 2Met$^+$), and biprotonated form (Met^{2+}). An initial survey of various adsorption modes was conducted to analyze how neutral or negatively charged xerogel interacts with neutral, monoprotonated, and biprotonated metformin molecules. This systematic study considered multiple potential adsorption modes, and the optimization of adsorption energies was initially performed in the gas phase. Subsequently, the most stable gas-phase geometries were considered as the initial point for the optimization, considering the effect of the solvent (aqueous phase).

The adsorption energy (E$_{ads}$) of metformin (MET) on the xerogel model was determined using the formula E$_{ads}$ = E$_{MET\text{-}surface}$ − (E$_{MET}$ + E$_{surface}$), where E$_{MET\text{-}surface}$ represents the total energy of the complex MET and the xerogel, E$_{MET}$ is the total energy of the metformin, and E$_{surface}$ is the total energy of the xerogel.

3. Results and Discussion

3.1. Xerogel Obtention Process

The polymerization mechanism of xerogels using NaHCO$_3$ as a catalyst to accelerate the polymerization is shown in Figure S3 [4,10]. The reaction begins with the species R$^-$ (resorcinol anion), which exhibits greater reactivity than its neutral counterpart. Subsequent stages involve addition reactions occurring at the 2, 4, and 6 positions of the aromatic ring of resorcinol, resulting in 2,4-bis(hydroxymethyl)benzene-1,3-diol species. This is followed by condensation, catalyzed by acid species, between hydroxymethylated species through hydroxyl groups, with water produced as a by-product. The resulting polyaromatic structures are interconnected by -CH$_2$- and -CH$_2$-O-CH$_2$ bridges. Monomers of R-F continue to condense, forming interwoven colloidal structures in coral-type systems.

3.2. Physicochemical Characterization of Xerogels

The FT-IR spectra of the samples with R ratios of 0.05, 0.10, 0.25, 0.30, and 0.40 are shown in Figure 2. All xerogel spectra present bands around 3410 cm^{-1}, indicating the presence of -OH groups that remain after the polymerization process. The band at 3172 cm^{-1}, corresponding to the phenolic -OH groups, disappears as the polymerization progresses and is related to the increase in the R:F ratio [11]. The bands observed between 3000 and 2775 cm^{-1} indicate the presence of stretching of the C-H bonds in the resorcinol molecule. Specifically, C-H stretches in aromatic compounds typically appear in this range [11]. The decrease in its intensity indicates an advance in the degree of polymerization. The disappearance of bands between 2643 and 2497 cm^{-1}, associated with resorcinol, suggests that phenolic -OH groups are decreasing due to substitution reactions in additions, as illustrated in Figure 2. Furthermore, bands in the 685 to 461 cm^{-1} range disappear due to the substitution of aromatic rings in resorcinol during these addition mechanisms, specifically denoting C-C backbone vibrations [11]. The appearance of new peaks between 2166 and 1704 cm^{-1} and between 1294 and 1017 cm^{-1} indicates the formation of ether groups (-C-O-C-), resulting from the condensation of polymeric monomers during the reaction (bond stretching between monomers) [12]. The bands in the 1135 to 950 cm^{-1} range represent C-H deformations of formaldehyde derived from its addition in the polymerization process. The band at 1612 cm^{-1} corresponds to ring stretching vibrations (C=C), while the bands between 1440 and 1374 cm^{-1} are associated with C-H bending vibrations. [13]. The blue zone in the FT-IR of Figure 2 presents stretch bands around 3300–2500 cm^{-1}; this is due to phenolic hydroxyl groups in resorcinol, residual unreacted hydroxyl groups during polymerization, and water adsorbed in the xerogel [11]; in Figure 2 (yellow area) are present in C=O stretching bands around 1760–1730 cm^{-1} [12].

Acidic and basic sites on an adsorbent material confer selectivity in the adsorption of specific compounds. While acidic sites may preferentially adsorb basic molecules, basic sites may be more likely to interact with acidic substances. Total acid sites and total basic sites are found from the calculation of the titration stoichiometry obtained. These results are shown in Figure S4; a concentration of total acid sites from 1.69 to 3.21 meq/g and total basic sites from 2.04 to 2.79 meq/g were obtained. The xerogel surface is acidic for R:F-0.05 because it presents 57% more acidic sites. For xerogel R:F-0.10, the surface presents a surface balance of acidic and basic sites as a difference of sites of 6.8% is found. R:F-0.25, R:F-0.30, and R:F-0.40 materials present surfaces with a greater proportion of basic sites, 62, 75, and 30%, respectively. The decrease in phenolic sites as the R-F ratio increases indicates that the degree of polymerization is directly proportional as the R-F ratio increases. This is because the phenolic groups of resorcinol are sites where the addition reactions described in Figure 2 occur.

Analyzing the surface charge lets us estimate the zero charge point of a material. The point of zero charge is a characteristic property of solid surfaces and represents the pH at which the material's surface has no net electric charge. For the xerogels analyzed, zero charge points of 6.51, 6.85, 6.93, 7.57, and 9.02 were obtained for the molar ratios of R:F 0.05, 0.1, 0.25, 0.30, and 0.40, respectively. R:F-0.30 and R:F-0.40 have slightly basic and one considerably basic loading points. This property is associated with the excess -OH ions from the resorcinol reaction system. R:F-0.40 has an enriched system of hydroxyl groups derived from adding formaldehyde to the polymeric structure, indicating a higher degree of reaction. At a more basic pH, the adsorption process of metformin from the xerogels will be more efficient because hydrogen bond interactions will be promoted between the hydroxyl groups of the xerogels and the amino groups of metformin.

The X-ray diffraction (XRD) pattern of xerogels with R-F ratios ranging from 0.05 to 0.40, depicted in Figure S5, reveals a distinct halo within the 16 to 20° (2θ) range, indicating their amorphous nature [14]. The particle size of sub-micrometer particles based on diffraction patterns was calculated using the Scherrer equation (Equation (S1) in the Supplementary Materials). The xerogels analyzed exhibited particle sizes ranging from 0.2523 nm to 0.2267 nm across the R:F ratio range. Notably, higher R:F ratios correlate

with smaller particle sizes, suggesting that an elevated R:F ratio promotes the formation of nucleation sites to a greater extent, thus facilitating a more uniform distribution of the reaction system throughout the material. The analysis of interlaminar space in the xerogels indicates no trend in the interlaminar space concerning the variation in R-F ratios (see the Supplementary Materials).
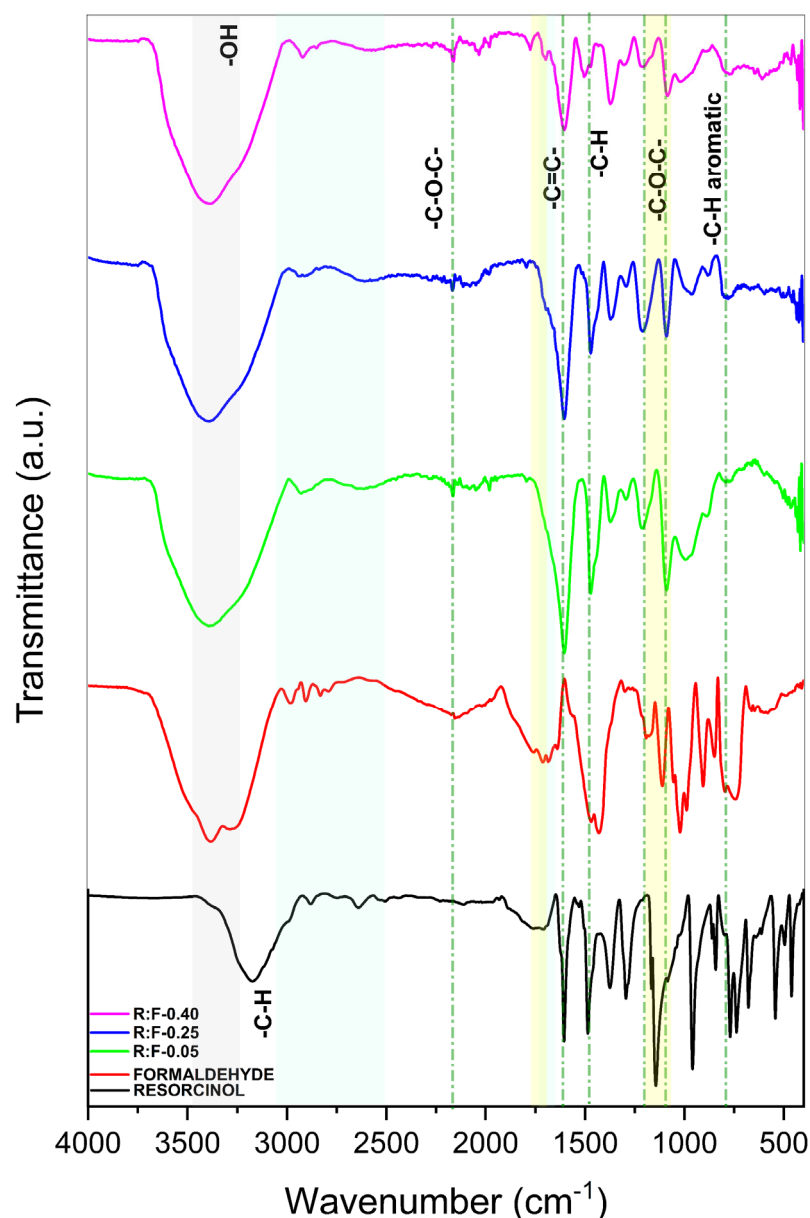
Figure 2. Infrared spectra of xerogel synthesis precursors and xerogels R-F-0.05, R-F-0.25, and R-F-0.4 (0.05, 0.25, and 0.40 R:F molar ratios, respectively).

SEM analysis showed that the excess of monomers contributes to the formation of larger particles because a greater number of monomers affects the reaction rate and kinetics of the process, promoting the agglomeration and coalescence of the particles, resulting in less homogeneous and larger particle distributions, as seen in Figure 3. Further, the observed morphology is agglomerated in irregular shapes with smooth and striated faces. The presence of striations in the agglomerates is attributed to the crushing process. Regular cutting striations are observed for the three xerogels analyzed; this is commonly attributed to materials with ordered and repetitive nucleation processes, so the polymerization system for the three systems has the same nucleation system. Figure 3 shows that increasing the R-F ratio leads to

larger particle sizes: 67.97 μm for R:F-0.05, 80.94 μm for R:F-0.25, and 95.52 μm for R:F-0.40. An increased R-F ratio makes more monomers available for xerogel particle formation, leading to a more extensive nucleation and growth during synthesis. Additionally, EDX (Figure 3) analysis makes detecting the significant presence of C, O, and Na possible. Hence, considering C and O, for R:F-0.05, weight proportions of 53.96% and 30.89% are obtained, respectively, while for R:F-0.40, the proportions are 68.05% and 38.11%, the above is following the increase in R-F ratios that contribute to the formation of more intermediates in the polymerization process and allow the condensation of extensive polymeric systems, made up of C and O because the precursors (R-F) are mostly made up of these elements. The EDX also shows the presence of Na, attributed to the catalyst, having 9.09% by weight and 1.84 for R:F-0.05 and R:F-0.40, respectively. The low quantity of Na in R:F-0.40 indicates that for the polymerization process of the xerogels at higher R-F ratios, a greater contribution from the catalyst is needed to begin the R and F addition process.
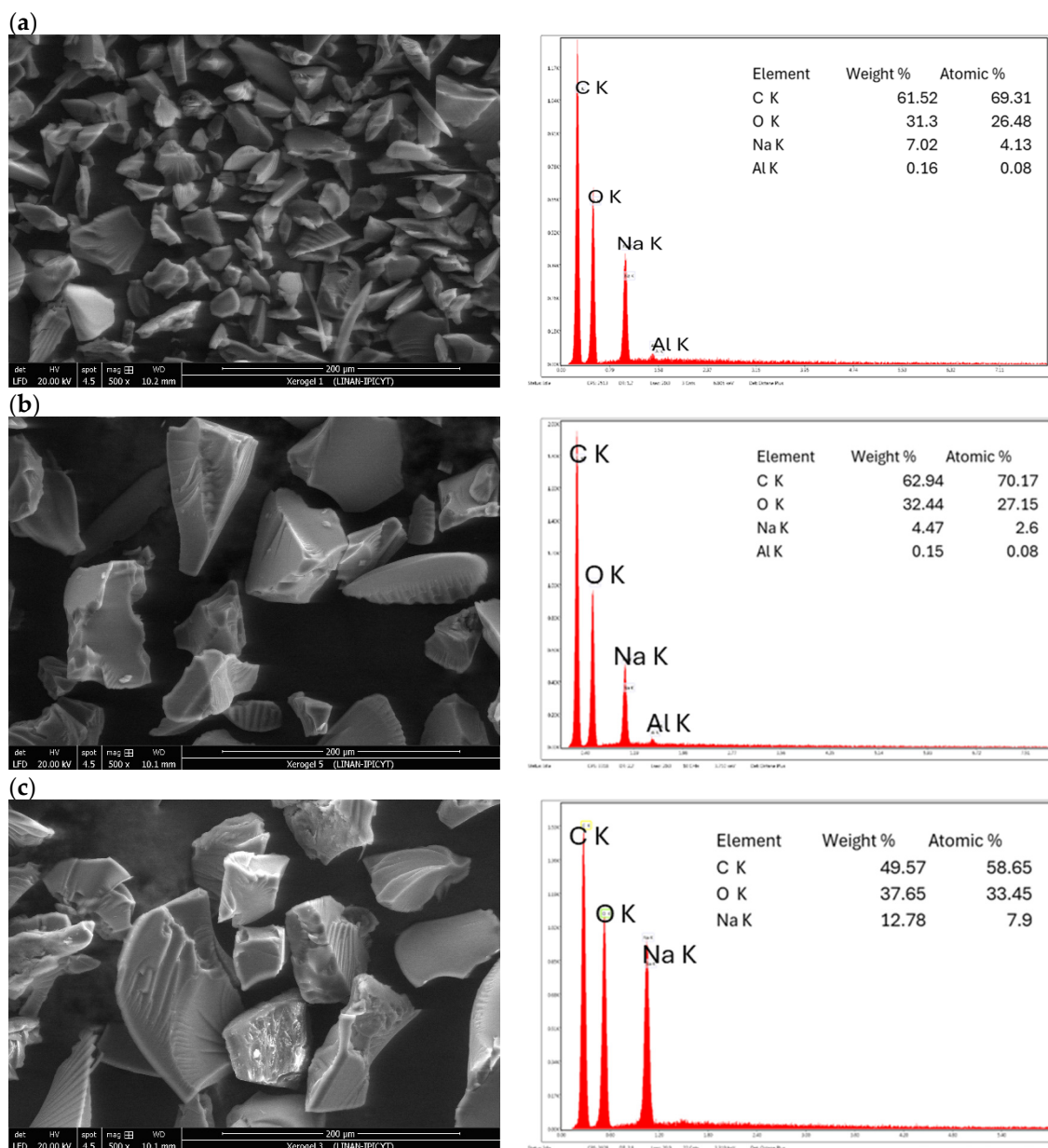
Figure 3. SEM micrographs and EDS analysis for particle size analysis, result of the variation in the molar ratio of R-F for the xerogels (**a**) R:F-0.05, (**b**) R:F-0.25, and (**c**) R:F-0.40, respectively.

The TEM micrographs show the agglomeration of the R-F xerogel particles (see Figure 4). The formation of nanometric aggregates is evident in all the samples examined. The size of the R:F-0.05 aggregates ranges from 6 to 202 nm, R:F-0.25 from 30.5 to 642 nm, and R:F-0.40 from 10 to 166 nm. The morphology of the aggregates for the R:F-0.05 and R:F-0.25 systems appears as grains around 100 nm (Figure 4a–e,g), but at sizes close to 10 nm, they resemble crystals (Figure 4h). Additionally, the R:F-0.05 system exhibits graphitized crystals (Figure 4b) that are 107 nm long. All the xerogels analyzed consist of granules corresponding to amorphous particles and graphitized sections [15]. The R:F-0.05 system has graphitized sections with an interlaminar space of 0.51 nm, for R:F-0.25 of 0.49 nm, and for R:F-0.40 of 0.52 nm. These findings are consistent with the interlaminar spaces identified in the XRD analysis.
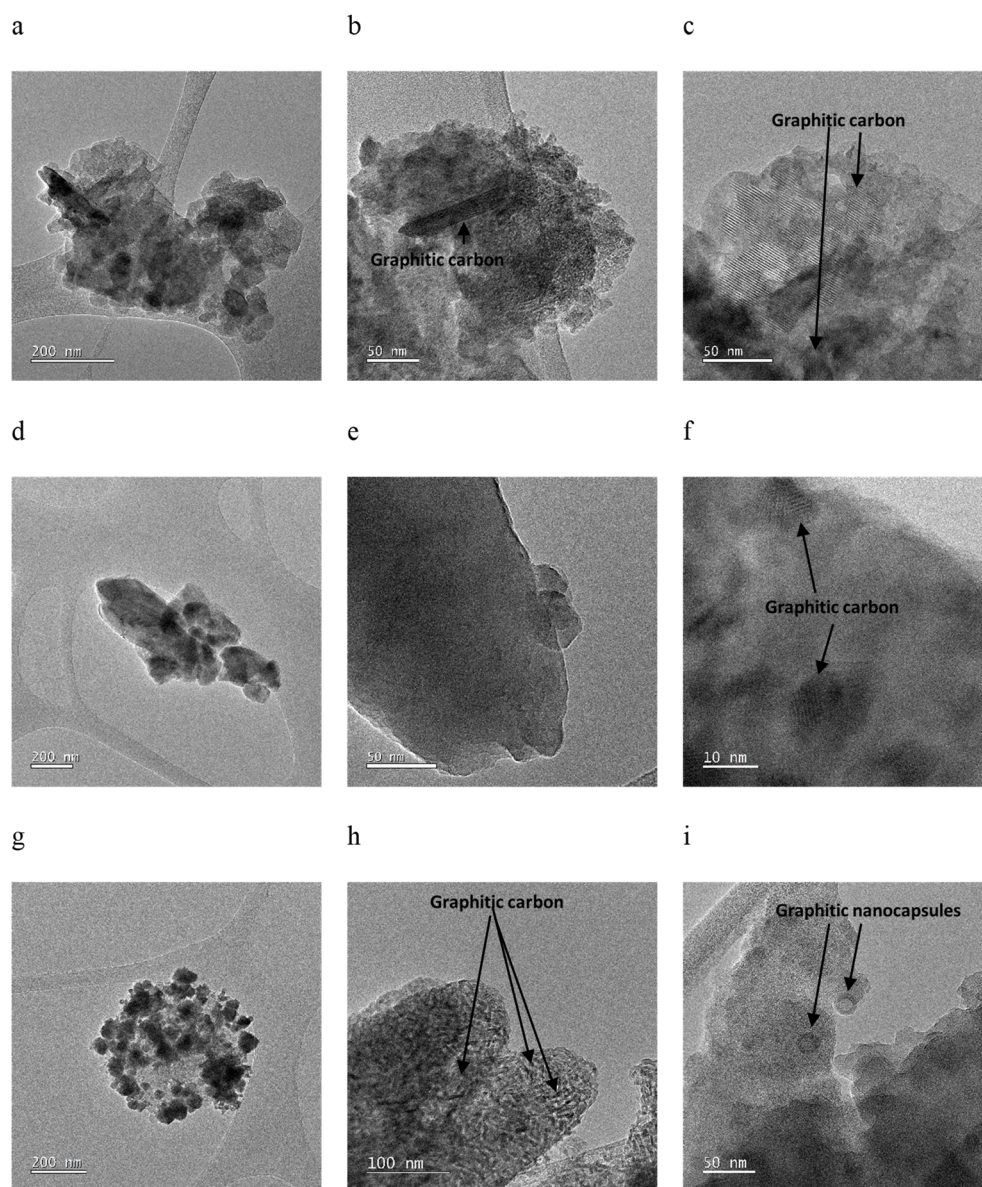
Figure 4. TEM figures of the internal morphology of the xerogels of R:F-0.05 (**a–c**), R:F-0.25 (**d–f**), and R:F-0.40 (**g–i**).

As the R:F ratio increases, the carbon content in the xerogel structure also rises. However, XRD analysis shows that the interlaminar space does not correlate with R:F ratio variations. Despite this, there is a relationship between the degree of graphitization and crystallinity. Polymers with a high concentration of carbon–carbon bonds tend to ex-

hibit greater graphitization [16]. The synthesized xerogels, characterized by a carbon-rich structural chemistry, align with this tendency. The pressure within the reaction systems stabilized the carbon structures of the xerogels, promoting the formation of denser or more ordered graphitized carbon structures. This stabilization enhanced the reorganization of carbon atom bonds within the xerogel structure, facilitating crystalline forms [17]. As the R:F ratio increases, more defined crystalline structures will be achieved. Figure 4 illustrates that the degree of crystallization and graphitization increases with higher R-F ratios. Specifically, Figure 4h,i show that the sample with an R:F-0.40, having a higher carbon content, presents extensive zones of graphitization and well-defined raw crystalline structures. Notably, this sample achieves graphitic nanoencapsulation, where carbon is organized into graphitic layers on a nanometer scale [18].

3.3. Adsorption Equilibrium

Studying adsorption equilibria in batch systems provides insights into the maximum adsorption capacities under specific conditions, such as temperature, pH, and initial concentration conditions. The adsorption capacity of these materials can be evaluated by varying the initial metformin concentration in the adsorption process using xerogels. As depicted in Figure 5, an increase in the initial metformin concentration leads to higher adsorption capacities irrespective of the R:F ratio. This behavior indicates that more contaminant molecules can be adsorbed onto the adsorbent at higher initial concentrations until reaching saturation.
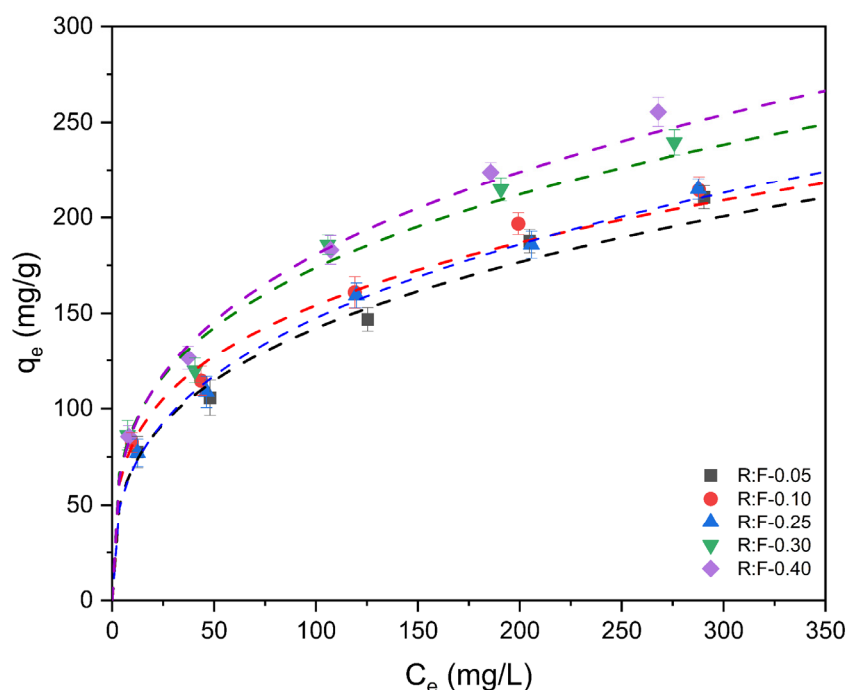
Figure 5. Evaluation of the adsorption capacity of metformin in R:F-0.05, R:F-0.10, R:F-0.25, R:F-0.30, and R:F-0.40, variation in the initial concentration of metformin from 50 to 500 mg/L, at pH 7 and 25 °C for seven days. q_e (mg/g, concentration of metformin adsorbed at equilibrium) and C_e (mg/L, metformin concentration at equilibrium).

The adsorption isotherms obtained from all the experiments were fitted to the Langmuir, Freundlich, and Prausnitz–Radke models, and the adjustments can be found in Table S1 (in Supplementary Information), considering Equations (2)–(4). According to the Langmuir model, the maximum adsorption capacities obtained were 206.6, 213.2, 229.2, 244.2, and 260.4 mg/g for R:F ratios of 0.05, 0.10, 0.25, 0.30, and 0.40, respectively. The rise in the adsorption capacity as a function of the R:F ratio could be explained according to the pH solution, metformin ionization, and pH_{PZC} of the xerogel adsorbents.

The adsorption process was conducted at pH 7, implying the presence of cationic forms of metformin (Figure S1). The point of zero charge for the xerogels with R:F ratios of 0.05, 0.10, and 0.25 is below the working pH ($pH_{solution} < pH_{PZC}$). Consequently, the material surface will be positively charged. For these xerogels, the adsorption mechanisms involve the formation of hydrogen bonds between the hydroxyl groups of the xerogels and the amino groups of metformin. For R:F ratios of 0.30 and 0.40 ($pH_{solution} > pH_{PZC}$), the adsorption mechanism implies hydrogen bond formation, but also electrostatic attractions are favored between the negatively charged surface xerogel and the positively charged metformin species in solution. The adsorption of metformin on the R:F-0.40 xerogel was confirmed by FT-IR analysis (Figure S6). The hydroxyl groups show a broad adsorption band in the 3400–3600 cm^{-1} region due to the O-H bond. This band exhibits lower intensity and a shift towards lower wavenumbers, suggesting the formation of hydrogen bonds (O-H····N) since the strength of the initially free O-H bond weakens when it becomes part of the O-H····N bond (Figure S6) [19,20]. In addition, the band at 1769 cm^{-1} indicates the interaction of the hydroxyl groups with the amino groups (NH····OH) [21]. On the other hand, the amino groups of metformin exhibit characteristic adsorption bands at 3342 cm^{-1} (N-H stretching), 1599 cm^{-1} (primary amine), and 1369–1417 cm^{-1} (C-N bond). As the metformin concentration increases, these bands are shifted to lower wavenumbers (3400–3600 cm^{-1}), suggesting the formation of electrostatic interactions between the xerogel surface and metformin molecules. These interactions can influence the stability of the adsorbed layer, the specificity, and the increase in adsorption energy during the adsorption process of metformin molecules. Therefore, the adsorption process onto the xerogel surface is governed by the occurrence of hydrogen bond formation at $pH_{solution} < pH_{PZC}$, while both electrostatic attractions and hydrogen bond formation are favored at $pH_{solution} > pH_{PZC}$.

The synthesized xerogel, R:F-0.40, demonstrates an impressive adsorption capacity of 325 mg/g, for removing metformin from aqueous solutions. This represents a 115.13% increase compared to the highest value previously reported in the literature, 151.07 mg/g, as shown in Table 2.

Table 2. Comparison of R:F in removing metformin compared to other literature.

Adsorbent	Adsorption Capacity (mg/g)	Experimental Conditions (Dose, Concentrations (C0), Time, Temperature, and pH	Potential Mechanisms	Reference
Graphene oxide	96.7	0.5 g/L, 8–40 mg/L, 25 °C, 160 min, 6	π–π interactions and hydrogen bonds	[22]
Graphene oxide	122.6	0.13 g/L, 300–700 mg/L, 3 h, 20.53 °C, 6.26	-	[23]
Molecularly imprinted polymers	80.0	1.0 g/L, 0–100 mg/L, 6 h, 25 °C, 10	Electrostatic attractions	[24]
Activated carbon from Sibipiruna	103.83	1.0 g/L, 25–900 mg/L, 6 h, 30–50 °C, 6	Physisorption	[25]
Hydrochar activated from *Byrsonima crassifolia* stones	113.6	2.5 g/L, 100–1000 mg/L, 7 days, 25 °C, 7	Attractive electrostatic interactions	[26]
Gum ghatti-cl-poly(N-isopropyl acrylamide-co-acrylic acid)/ CoFe$_2$O$_4$ nanocomposite hydrogel	151.07	0.8 g/L, 25–250 mg/L, 24 h, 30 °C, 8	Lone pair–pi interaction, electrostatic interactions, and hydrogen bonding	[27]
Resorcinol-Fomraldehyde xerogels	325	0.5 g/L, 50–500 ppm, 7 days, 25 °C, 11	Electrostatic interactions, and hydrogen bonding	This study

3.3.1. Effect of pH

The relationship between pH and adsorption capacity is analyzed using experiments in which the pH of a solution is varied, and the number of contaminants adsorbed by the material is monitored, as shown in Figure 6. The pH affects the surface charge of the adsorbent material due to the ionization of the functional groups on its surface. It can modify the adsorbent's affinity for the contaminants present in the solution. Figure 6 indicates that, in general, the adsorption capacity of xerogels increases as the R:F ratio rises. This increase is attributed to structural hydroxyl groups that enable hydrogen bond interactions. Additionally, the adsorption capacity also rises with increasing pH due to electrostatic interactions between the surface charge of the xerogels, which is influenced by their isoelectric points, and the cationic forms of metformin. A pH of 3 results in a positively charged surface ($pH_{solution} < pH_{PZC}$) and positively charged metformin (dicationic form, as shown in Figure S1) for all the xerogels used. This causes electrostatic repulsion between the adsorbent and the metformin, significantly decreasing the adsorption capacity. At this pH, the maximum adsorption capacity for all xerogels does not exceed 50 mg/g, and the interaction forces are primarily due to hydrogen bonds. The electronegativity of oxygen in the xerogel's hydroxyl group is high, creating an electron negative charge (δ-) on the oxygen atom and a low electron charge (δ+) on the hydrogen atom. This polarity facilitates an attractive interaction between the hydroxyl group's oxygen atom and the mono-cationic metformin's hydrogen atom. Changing the pH of the solution in the adsorption process from 3 to 7 improves the adsorption process by 200, 332, 282, 221, and 271% for R:F 0.05, 0.10, 0.25, 0.30, and 0.40, respectively. At pH 3, the hydroxyl group of phenol will be predominantly in its protonated form. Conversely, at pH 7, they become partially ionized (phenolates), as indicated by the xerogels' isoelectric points. The change in pH from 3 to 7 influences the charge and polarity of hydroxyl groups, affecting metformin's adsorption capacity. Then, this ionization facilitates electrostatic interactions between the hydroxyl groups and metformin, thereby promoting metformin adsorption.

Additionally, XRD analysis of particle size (see Supplementary Materials) reveals a trend where the particle size decreases with increasing R:F ratio, significantly reducing adsorption sites' steric availability. For R:F-0.40, despite having the smallest particle size among all xerogels, the increase in adsorption capacity is not substantial concerning R:F-0.30. It is primarily due to its isoelectric point being 9.02, which limits the availability of phenolates crucial for generating electrostatic interactions. Moreover, further elevating the pH from 7 to 11 results in a more modest improvement of 21% to 54% in adsorption efficiency. The maximum adsorption capacity occurs at a pH of 11, with R:F-0.40 reaching 329 mg/g values, as shown in Figure 6. At this pH, the adsorption capacity increases due to reduced electrostatic repulsion and enhanced interactions between the xerogels and metformin molecules. At a pH of 11, all xerogels are already above the isoelectric point, and all active sites are negatively charged (hydroxyl groups can be deprotonated in a basic environment), so the surface charge of the xerogel is negative, and the metformin species is neutral. This condition led to the formation of hydrogen bonds between the amino groups of metformin and the hydroxyl groups of the xerogel. In the case of amino and hydroxyl groups, these bonds form due to the differences in electronegativity between the atoms (NH····OH) involved and the ability of hydrogen atoms to form attractive interactions with the electron pairs of electronegative atoms [28]. Hydrogen bonds play a crucial role in the main interactions between the adsorbent surface and the adsorbate, enhancing adsorption [29]. Hence, the pH of a metformin solution plays a crucial role in adsorption processes, affecting the adsorbent's surface charge, the adsorbate's charge, the type of interactions involved, and the overall efficiency of the process.

The analysis of the xerogel (R:F-0.40) with metformin allows us to determine its actual adsorption capacity and understand how the adsorbate interacts with the surface of the adsorbent. Characterization techniques provide detailed information on the physical, chemical, and structural properties of the adsorbent and its interaction with the adsorbate.

As described above, the interactions found for all xerogels with metformin are due to hydrogen bonds between the xerogel's hydroxyls and the metformin's amino groups.
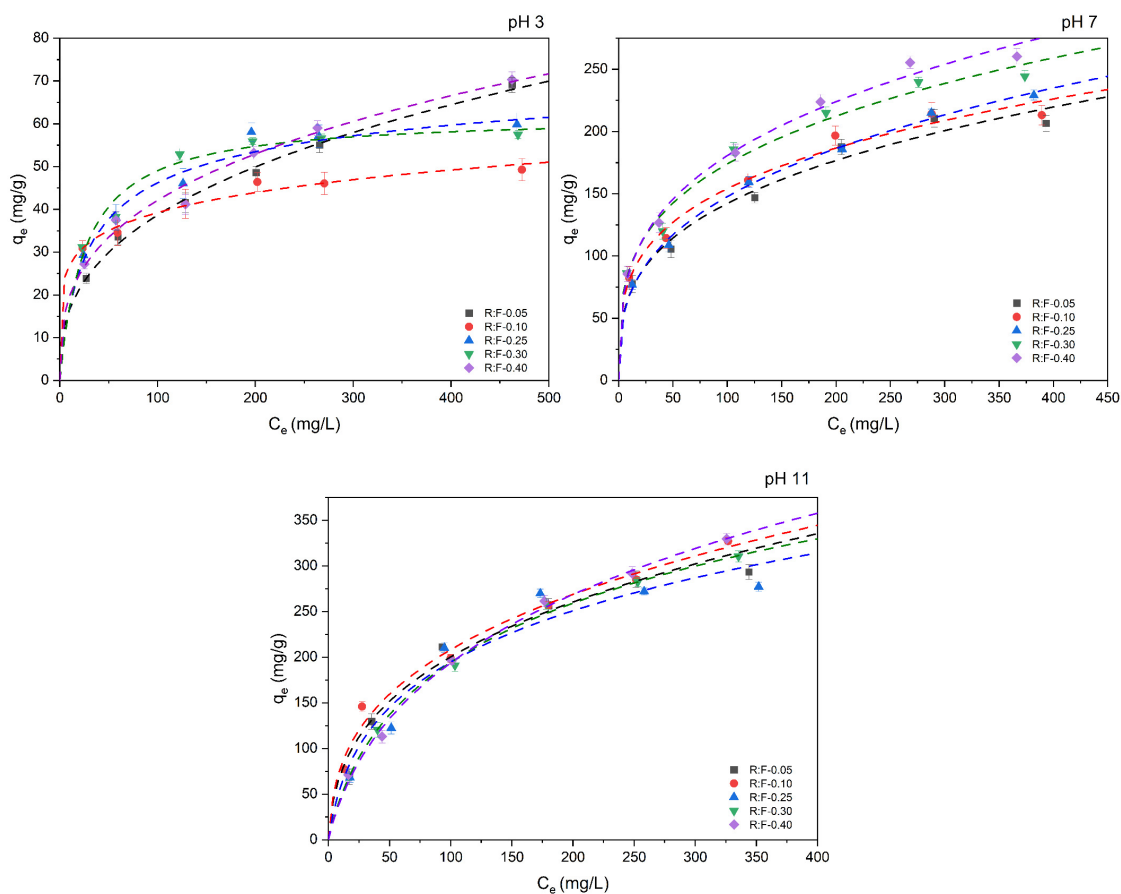
Figure 6. Adsorption equilibrium as a function of the solution pH, and there is a variation in the initial concentration of metformin from 50 to 500 mg/L and 25 °C for seven days.

SEM analysis shows the surface morphology of R:F-0.40 after metformin adsorption, in Figure 7 *and* Figure S7. The structure of the xerogel does not present modifications due to the adsorption process; only the accumulation of cubic crystalline structures dispersed on the surface of the xerogel is denoted. With the EDS analysis (Figure 7), it is possible to determine that the deposited crystals are mainly made up of N (6.78% w) and Cl (9.13% w). Element mapping analysis in crystals with metformin is feasible to analyze with the chlorine that is present in metformin (1,1-Dimethylbiguanide hydrochloride) at 21.4% w because the identification of nitrogen is complicated due to the characteristic energy emitted by nitrogen's X-ray electrons being relatively low, which can make it difficult to detect and distinguish it from other elements. As shown in Figure S7, the mapping for chlorine allows us to visualize a uniform surface distribution of metformin in R:F-0.40. The metformin adsorption analysis is complemented with a TGA analysis (Figure S8), which provides information on the thermal stability of the R:F-40/Metformin system at different temperatures, with a shift in the thermogram to better thermal stability to degradation because the amount of mass loss is improved by between 4 and 13%. TGA analysis confers relevance to molecular interactions between xerogel and metformin since it significantly changes the mass loss rate compared to xerogel alone. Figure S8 shows a considerable mass loss between 265 and 325 °C, related to the loss of $-CH_3$ and $-NH_2$ groups from the original molecule ([30]). The R:F-0.40/Metformin sample was loaded with a solution at 80 mg/L, which had an equilibrium concentration of 36.5 mg/L, and with equilibrium calculations, it is expected to have 135.94 mg/g (13.59 wt. %) of adsorbed metformin. When analyzing Figure S8, integrating the areas under the curve for the loaded and unloaded

sample, 46,219.79 and 40,886.61 units are found, respectively, so there is a metformin mass of 13.04 wt. %. That indicates that the experimental equilibrium results are consistent in adsorbed metformin when analyzed using the TGA technique.
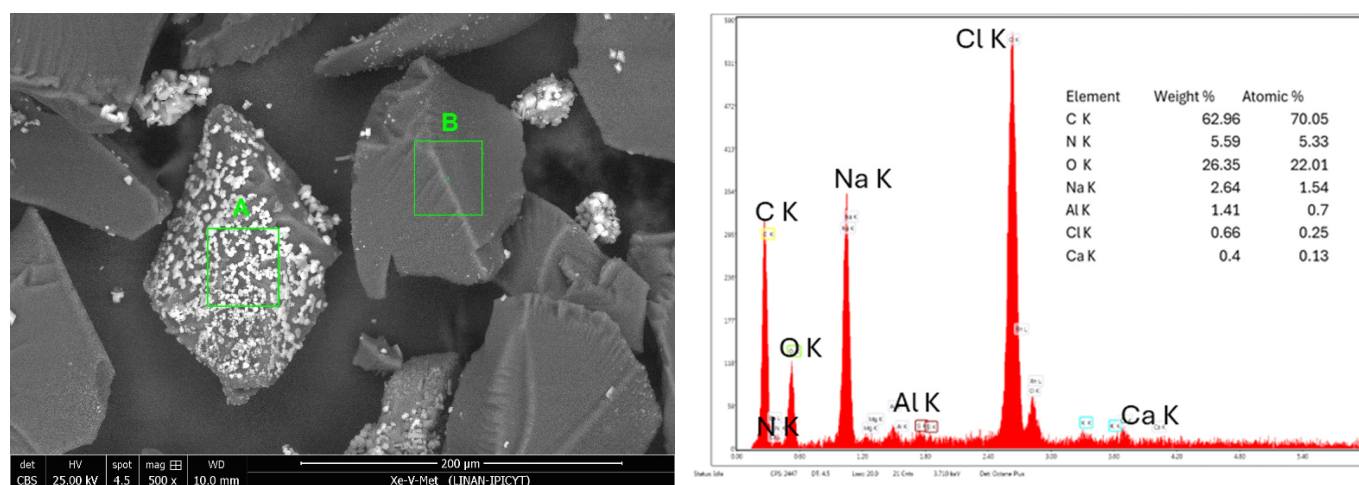
Figure 7. SEM and EDS in recovered R:F-0.40 after seven days of metformin adsorption at 80 mg/L, pH 7, 25 °C.

3.3.2. Effect of Temperature and Thermodynamic Analysis

The variation in temperature of a solution in an adsorption process can impact the metformin adsorption capacity of xerogels. In conjunction with the pH variation study, the temperature effect provides insights into the adsorption behavior and the underlying interactions between metformin and the xerogel adsorbents. Three different R:F ratios (low, intermedia, and high) were selected to study the effect of temperature on the adsorption process. As shown in Figure 8, increasing the temperature for R:F 0.05, 0.25, and 0.40 directly enhances the amount of metformin adsorbed. Increasing the temperature can enhance the diffusion of molecules to the adsorption sites and increase the adsorption probability. At higher temperatures, molecules typically experience an elevation in kinetic energy. This heightened thermal energy facilitates the diffusion of adsorbate molecules toward the adsorption sites on the adsorbent. Consequently, they engage more effectively with the surface of the adsorbent, enhancing interaction and promoting adsorption. As a result, more adsorbate molecules can be adsorbed, having a maximum adsorption capacity of 267 mg/g for R:F-0.40. For the xerogels analyzed in Figure 8, the increase in temperature from 15 to 25 °C improves the adsorption capacity between 11% and 22%. In contrast, the increase from 25 to 45 °C improves the adsorption capacity between 2.5% and 11%. Considering these findings, it is crucial to analyze the operational costs of maintaining higher process temperatures to balance adsorption capacity and economic feasibility.

The metformin adsorption heat in xerogels was estimated using the Langmuir isotherm, K_L, equilibrium constant values and applying the following graphical Equation (6):

$$\ln(K_L) = -\frac{\Delta H_{ads}}{R}\left(\frac{1}{T}\right) \tag{6}$$

where:

- ΔH_{ads} = Adsorption heat, J/mol.
- K = Langmuir isothermal equilibrium constant related to adsorption enthalpic, L/mg.
- R = Universal constant of ideal gases, 8.314 J/mol K.
- T = Temperature, K.
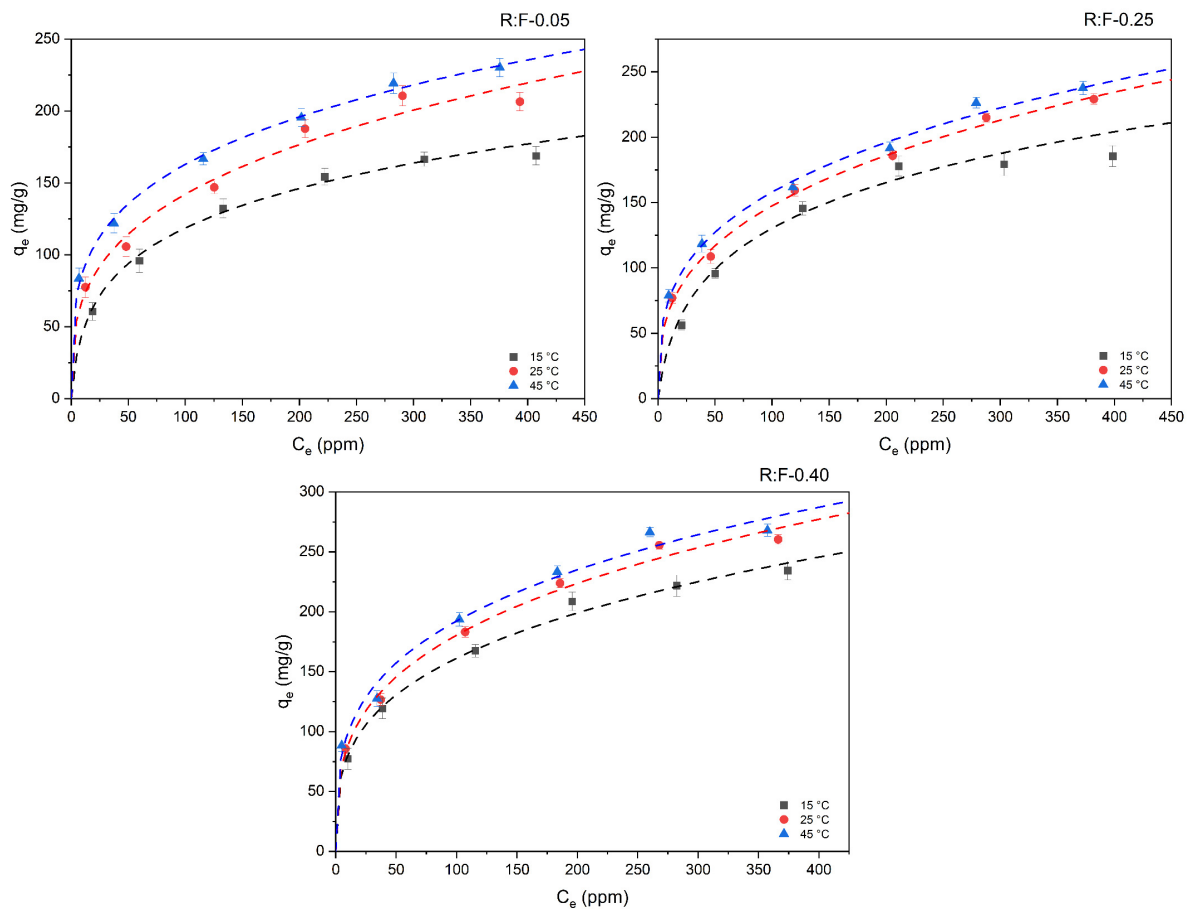
Figure 8. Evaluation of the adsorption capacity of metformin in R:F-0.05, R:F-0.25, and R:F-0.40, variation in the temperature (15, 25, and 45 °C) of metformin solution, and initial concentration of metformin from 50 to 500 mg/L at pH 7 for 7 days.

As observed in Equation (6), the part $\frac{\Delta H_{ads}}{R}$ corresponds to the slope of the linear adjustment. The values of the free Gibbs energy (ΔG) and the entropy (ΔS) changes were calculated following Equations (7) and (8) [31].

$$\Delta G^0 = -RT\ln(K_L) \tag{7}$$

$$\ln(K_L) = -\frac{\Delta H_{ads}}{R}\left(\frac{1}{T}\right) + \frac{\Delta S^0}{R} \tag{8}$$

The thermodynamic parameters obtained for the metformin adsorption process onto the xerogel adsorbents are presented in Table 3. The positive enthalpy values ($\Delta H_{ads} > 0$) across all analyzed xerogels suggest that adsorption occurs through a physical and endothermic mechanism at 15, 25, and 45 °C. These results suggest that physisorption occurs during the metformin adsorption process. This physisorption is evidenced by hydrogen bonds between metformin molecules and xerogel surfaces, as indicated by low energy values (<40 kJ/mol) [32]. Additionally, it was observed that the ΔH_{ads} values decrease with increasing temperature, indicating that the metformin adsorption process onto the xerogels is favored with an increase in temperature. Furthermore, all negative free energy values (ΔG^0) indicate that the thermodynamic adsorption process is feasible and spontaneous from a thermodynamic perspective. Metformin molecules are attracted and attached to the surface of the adsorbent by favorable interaction mechanisms (at higher temperatures), such as hydrogen bonds or electrostatic interactions. The positive values of entropy changes (ΔS^0) imply an increase in the system's entropy attributed to metformin adsorption on the

surface of the xerogels, contributing to a favorable thermodynamic process. This adsorption process modifies the surface of the adsorbent, and metformin molecules have a specific molecular orientation and configuration.

Table 3. Thermodynamics of the adsorption of xerogels.

Xerogel	Temperature (°C)	ΔHads (kJ/mol)	$-\Delta G^0$ (kJ/mol)	ΔS^0 (J/mol)
R:F-0.05	15		9.41	
	25	19.33	9.47	34.45
	45		8.37	
R:F-0.25	15		9.84	
	25	12.86	9.72	10.50
	45		9.52	
R:F-0.40	15		8.60	
	25	0.77	9.05	27.16
	45		9.41	

3.3.3. Effect of Competitive Ions

Inorganic salts can significantly impact adsorption processes, influenced by the specific characteristics of the salts and the adsorbent materials. Primarily, salts in solutions alter the adsorption capacity of the adsorbent by blocking active sites or inducing structural changes in the material [33]. Notably, the R:F-0.40 adsorbent, with a substantial proportion of basic sites (2.31 meq/g) and a point of zero charge at 9.02, should be influenced by the presence of salts like $MgCl_2$, $CaCl_2$, and NaCl in the adsorption process of metformin due to the cations from these salts competing for the active sites (hydroxyl groups) in the xerogel surface. Figure 9 shows that the presence of Na^+ decreases the adsorption capacity of R:F-0.40 by 25–62%, Mg^{2+} by 70–73%, and Ca^{2+} by 59–78%. These decreases are due to coordination complexes between the aqueous ions and the basic sites of R:F-0.40. The hydroxyl groups promote these coordination complexes because the oxygen atoms of the hydroxyl groups donate unshared electron pairs to the metal cations, creating coordination bonds [34]. Furthermore, the ionic radius of Ca^{2+} (99 pm) is larger than that of Mg^{2+} (65 pm), meaning that the electrostatic compensation on the xerogel's basic sites will be greater for Ca^{2+}. Consequently, an increase in Ca^{2+} concentration more significantly reduces metformin adsorption. This is because Ca^{2+} forms coordination complexes, compounds formed by the interaction of a metal ion with a ligand, in this case, the hydroxyl groups on the xerogel. The larger ionic radius of Ca^{2+} (approximately 100 pm) compared to Mg^{2+} (approximately 72 pm) allows Ca^{2+} to interact more extensively with multiple hydroxyl groups, leading to a stronger and more extensive network of coordination complexes. This extensive interaction results in a more effective neutralization of the surface charge of the xerogel, causing a significant reduction in available active sites for metformin adsorption and creating steric hindrance as its concentration increases. Contrastingly, Mg^{2+}, with its smaller ionic radius, forms less extensive coordination complexes with the hydroxyl groups. This clear contrast with Ca^2 allows for greater accessibility of the adsorption sites for metformin molecules. As a result, while Mg^{2+} still competes with metformin for binding sites, it causes less steric hindrance and surface charge neutralization compared to Ca^{2+}. Therefore, increasing the concentration of Mg^{2+} to 0.5 M leads to a less significant decrease in metformin adsorption than Ca^{2+}. According to Table 2, the xerogels' metformin adsorption capacities are competitive, even with the effect of the salts used.
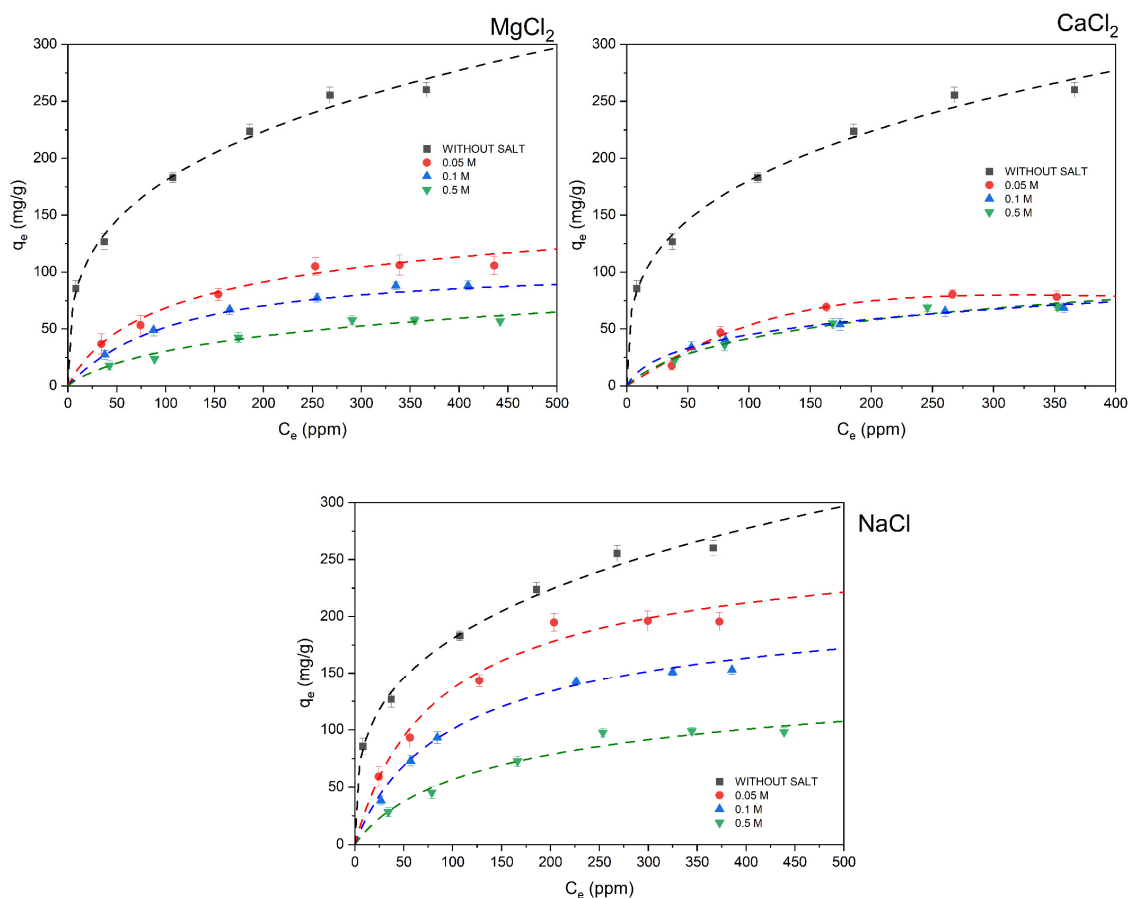
Figure 9. Analysis of the effect of 0.05, 0.1, and 0.5 M solutions of MgCl$_2$, CaCl$_2$, and NaCl on the adsorption isotherms of metformin in R:F-0.40, at 25 °C and pH 7.

3.3.4. Computational Results on the Adsorption of Metformin

DFT calculations have been instrumental in exploring various properties of carbon aerogels and xerogels, such as pore size distribution, pore volume in carbon aerogels, and surface areas [35]. Additionally, of note are the photothermal effects in graphene-CuFeSe$_2$ aerogels by simulating the influence of single-layer graphene on CuFeSe$_2$ clusters and in determining hydrogen bond lengths in reduced graphene oxide aerogel membranes, which revealed significant impacts on pore structure [36]. Furthermore, DFT has been utilized to analyze the hydrophobic mechanism in S and N co-doped graphene aerogels, attributing hydrophobicity to changes in surface electrostatic potentials, charge densities, and electron distribution resulting from co-doping [37]. Although the authors are unaware that DFT is being used to investigate antibiotic adsorption on xerogels specifically, computational tools have been extensively employed to model the adsorption processes of antibiotics on other materials [38]. These diverse applications underscore DFT's robust capability to elucidate the molecular-level properties of a wide range of materials. This study used computational calculations to investigate the possible interactions between metformin and the hydroxyl groups in the xerogels. According to the experimental results, the pH of the solution plays an important role in the adsorption of metformin on the surface of the xerogels. Therefore, molecular simulations were carried out to model the xerogel surface at three distinct pH levels: 2, 7, and 11. Different structural configurations (Tables S4 and S5) were proposed for these pH conditions based on the material's pH$_{PZC}$ values. Specifically, at pH = 2, a neutrally charged xerogel model (Xer) was considered; at pH = 7, both neutral and negatively charged xerogel models (Xer and Xer$^-$) were examined; and at pH = 11, a negatively charged xerogel model (Xer$^-$) was evaluated. In addition, considering the three pH values mentioned before and the speciation curve of metformin related to protonation–

deprotonation of metformin (see Supplementary Materials Figure S1), four different forms of metformin were considered: neutral form (Met), monoprotonated form (1Met$^+$ and 2Met$^+$), and biprotonated form (Met^{2+}). Therefore, the calculated adsorption energies (E$_{Ads}$) and geometry for the several proposed models are summarized in Tables S2, S3, and Figure S9. Considering different adsorption modes for the four forms of metformin, let us establish strong interaction-type hydrogen bonds and electrostatic attraction between protonated or deprotonated hydroxyl groups and amino groups with neutral, monoprotonated, and biprotonated metformin. The systematic study of the E$_{Ads}$ for all systems led to the conclusion that the adsorption is preferred over negatively charged xerogel and monoprotonated metformin pH = 7 and neutral metformin and negatively charged xerogel at pH = 11, since the metformin adsorption energy values were lower than those obtained for neutral xerogel and biprotonated metformin in all structures evaluated (Table S2). In this sense, high pH values favor metformin and xerogel interaction via the formation of electrostatic attraction and hydrogen bonds. These results agree with experimental results, which indicated that metformin adsorption is favored at high pH values. The stability of the different geometries can be deducted based on their E$_{Ads}$. Hence, for the most stable geometries, the solvent effect was considered to achieve a better approximation to real aqueous solutions, and the obtained results are reported in Figure 10 (see also Table S3). It can be observed that E$_{Ads}$ values decrease (become more negative) significantly under this approximation, ratifying the high favorability of metformin adsorption under these adsorption modes. The most stable adsorption modes for neutral, monoprotonated, and biprotonated are displayed in Figure 11. The E$_{Ads}$ for biprotonated, monoprotonated, and neutral metformin adsorbed onto xerogel are displayed in gas and aqueous phases. However, the calculated adsorption energies of metformin, accounting for implicit solvation effects, are significantly lower in magnitude compared to those obtained from gas phase interactions (See Table S3). Thus, including solvation effects notably impacts the adsorption energy values as previously reported for other systems [39]. It can be observed that for the most stable metformin adsorption modes onto xerogel structures, the geometries are established and stabilized through the formation of several hydrogen bonds and the electrostatic attraction between deprotonated hydroxyl xerogel groups and monoprotonated metformin.
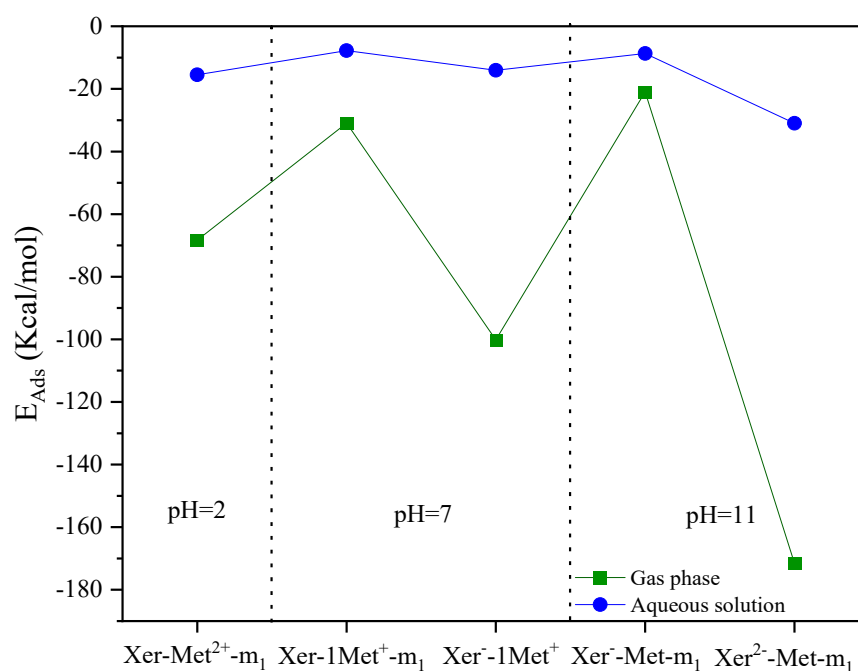
Figure 10. Adsorption energies (E$_{Ads}$) for the most stable models of biprotonated, monoprotonated, and neutral metformin adsorbed onto xerogel structure at three different pH values: 2, 7, and 11.

pH = 2

Xer-Met²⁺-m₁

pH = 7

Xer-1Met⁺-m₁

Xer-1Met⁺

pH = 11

Xer -Met-m₁

Xer²⁻ -Met-m₁
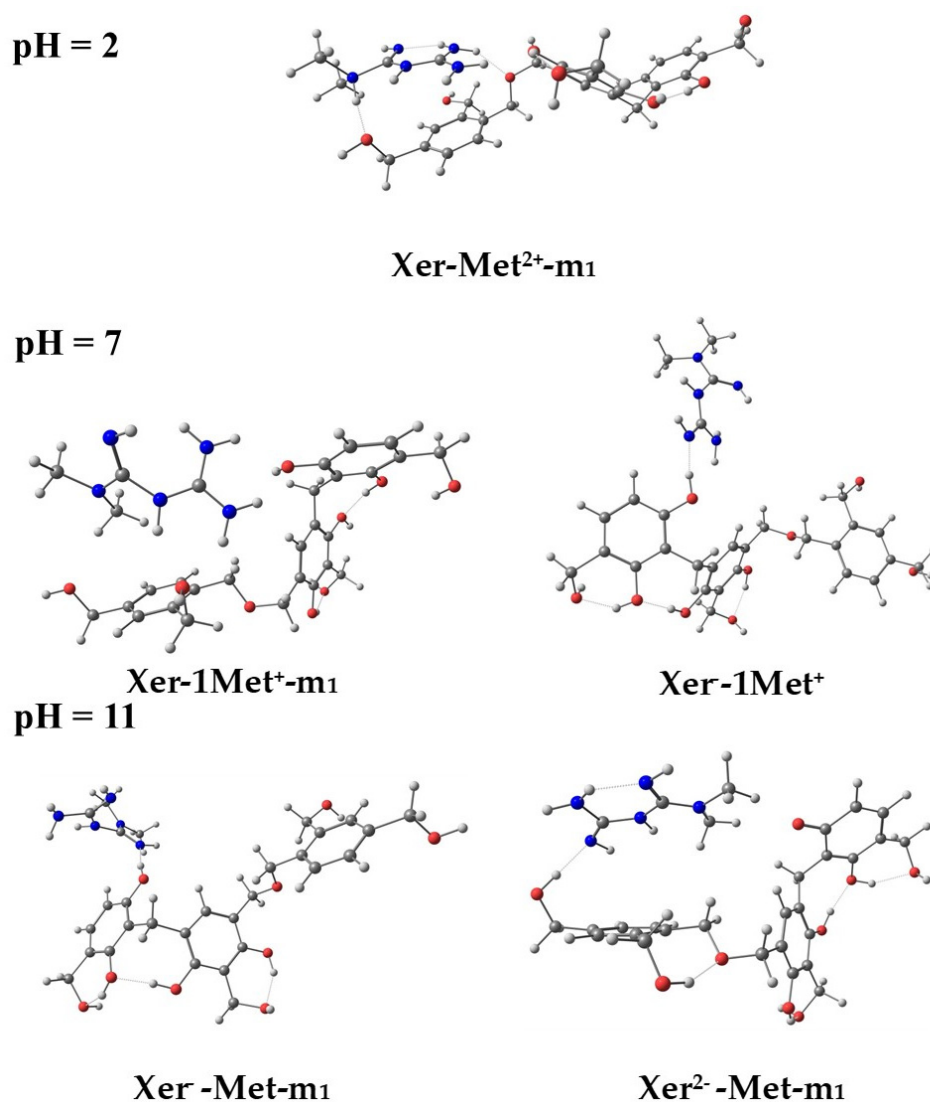
Figure 11. Most stable adsorption modes of metformin molecules on xerogels models. The C, O, H, and N atoms are symbolized by dark gray, red, white, and blue, respectively.

3.3.5. Adsorption in Simulated Urine

Analyzing the adsorption process of metformin in simulated artificial urine provides insights into the selectivity of the adsorbent. Simulated urine contains various chemical species that compete with metformin for adsorption sites on the adsorbent. By examining metformin adsorption in this context, it can evaluate the adsorbent's selectivity for metformin amidst other potential competitors in real-world scenarios. Figure 12 presents the evaluation of the xerogel adsorption capacity of R:F-0.40 in synthetic urea, and urine is presented. Synthetic urine, prepared with inorganic salts, urea, and creatinine, served as the dissolution medium for metformin at various concentrations (50 to 500 mg/L) to obtain the adsorption isotherm. The results showed a significant decrease in metformin adsorption capacity in R:F-0.40, from 260.40 mg/g to 99.26 mg/g (a 61.88% reduction) in the presence of urea and to 170.56 mg/g (a 34.5% reduction) in the presence of synthetic urine. The considerable decrease in metformin adsorption in competition with urea is attributed to urea occupying a greater proportion of the adsorption sites of R:F-0.40 due to its smaller molecular size, greater polarity, and ability to form hydrogen bonds between its primary amine groups of the urea and the hydroxyls of the xerogel. This interaction is illustrated in Figures S10 and S11, where the adsorption band at 3305 cm^{-1} is attributed to amine hydrogen bonds [40].
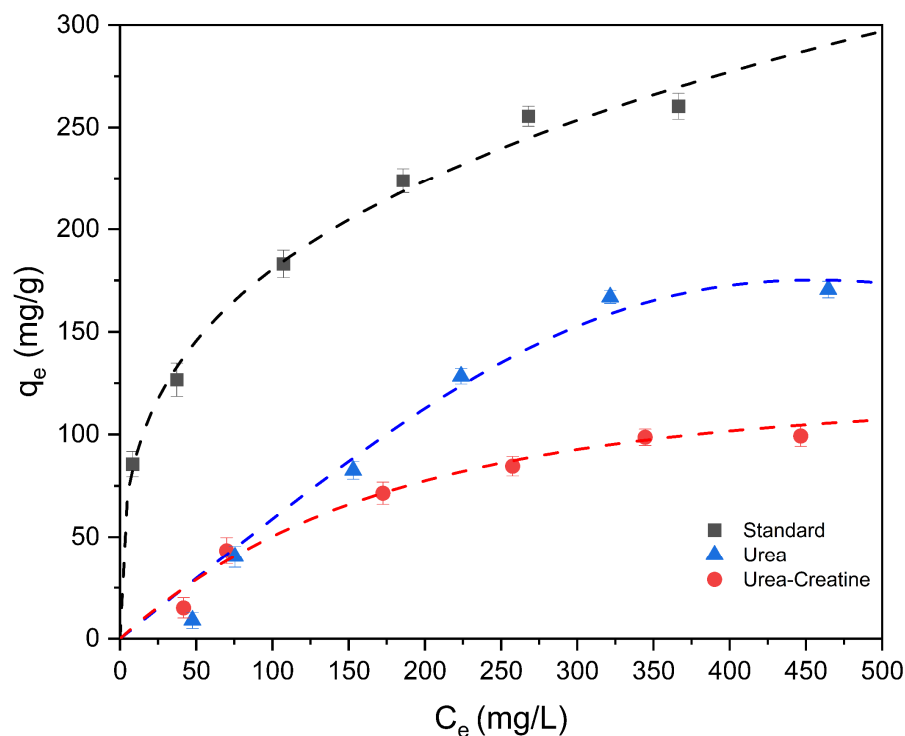
Figure 12. Evaluation of the adsorption capacity of metformin in R:F-0.40 with synthetic urea and urea–creatine urine, variation in the initial concentration of metformin from 50 to 500 mg/L at pH 7, 25 °C for 7 days. "Standard" is the adsorption process only with metformin in a variation of 50 to 500 mg/L at pH 7, 25 °C for 7 days.

For the two synthetic urines used, the adsorption bands between 3450 and 3150 cm^{-1} found in Figure S10 indicate the presence of amino groups in R:F-0.40, confirming the adsorption of urea and creatine. Creatine is a polar molecule due to the presence of amino and carboxyl groups, which facilitates its interaction with polar adsorbent surfaces such as R:F-0.40. Metformin is also a polar molecule due to the amino and amide groups, but it may have greater structural complexity (higher molecular weight and atomic dimensions) than creatine and urea, which may hinder its interaction with the adsorbent sites of the xerogel. Additionally, creatine forms hydrogen bonds, further enhancing its adsorption. While urea also forms hydrogen bonds, its greater structural complexity and the presence of two carbamide functional groups could affect the nature and strength of these interactions. Consequently, the system with metformin, urea, and creatine (Figure S11) will be more selective toward creatine adsorption. In Figure S12, the UV–vis adsorption bands of metformin (232 nm) are still visible after the adsorption process, indicating a decrease in adsorption capacity due to the competitive adsorption of the synthetic urine components. The adsorption bands of urea (192 nm) and creatine–urea (194 nm) in solution with metformin are not noticeable after the adsorption process, suggesting that the system completely adsorbs urea and creatine. Therefore, the adsorption of metformin onto R:F-0.40 decreases in the presence of these competing components.

3.3.6. Reuse Cycles

Reusing adsorbent materials reduces waste and more efficiently uses natural resources. Evaluating reuse cycles helps determine the durability and useful life of the material, which positively impacts environmental sustainability. The reusability of an adsorbent material significantly impacts its adsorption capacity due to material wear, loss of active sites, contaminant accumulation, changes in chemical structure, and regeneration effects. Figure 13 presents the impact of reuse cycles on the adsorption capacity of R:F-0.40, showing a notable decrease with each cycle. At pH 11, the adsorption capacity drops significantly by 73.23% (from 325 to 87 mg/g). At pH 7, the reduction is 52.31% (from 260 to 124 mg/g);

at pH 3, it is 38.57% (70 to 43 mg/g). Hence, low pH values affect adsorption capacity, resulting in minor adsorption. Balancing reusability and adsorption capacity, pH 7 proves optimal, maintaining an adsorption capacity of 124 mg/g in the third reuse cycle, which remains competitive with current materials (Table 2). Figure S13 shows that with increasing reuse cycles, the desorption capacity of R:F-0.40 decreases to 7.11%. This suggests that the electrostatic interactions and hydrogen bonds facilitating the adsorption process effectively retain metformin, thereby hindering its release from the polymeric structure during reuse cycles. As illustrated in Figure S14, after three reuse cycles, R:F-0.40 still exhibits amino group bands between 3150 and 3450 cm^{-1}. The adsorption band at 3151 cm^{-1}, associated with OH stretching due to hydrogen bonds, remains, while the band at 3412 cm^{-1}, corresponding to the hydroxyls of the initial polymeric structure, disappears [19]. This indicates that a significant amount of metformin remains immobilized inside the xerogel. The persistent presence of metformin after the adsorption cycles underscores the strong electrostatic interactions and hydrogen bonds between the adsorbate and the adsorbent material, suggesting a potential for irreversible adsorption. This retention highlights the efficiency of R:F-0.40 in immobilizing metformin, though it poses challenges for the material's reusability. Future work contemplates using different pH, temperature, and amount of extractant solvent conditions to improve the removal process of metformin from xerogels. It may also contemplate applications in controlled release systems for xerogels loaded with metformin, considering biological safety tests.
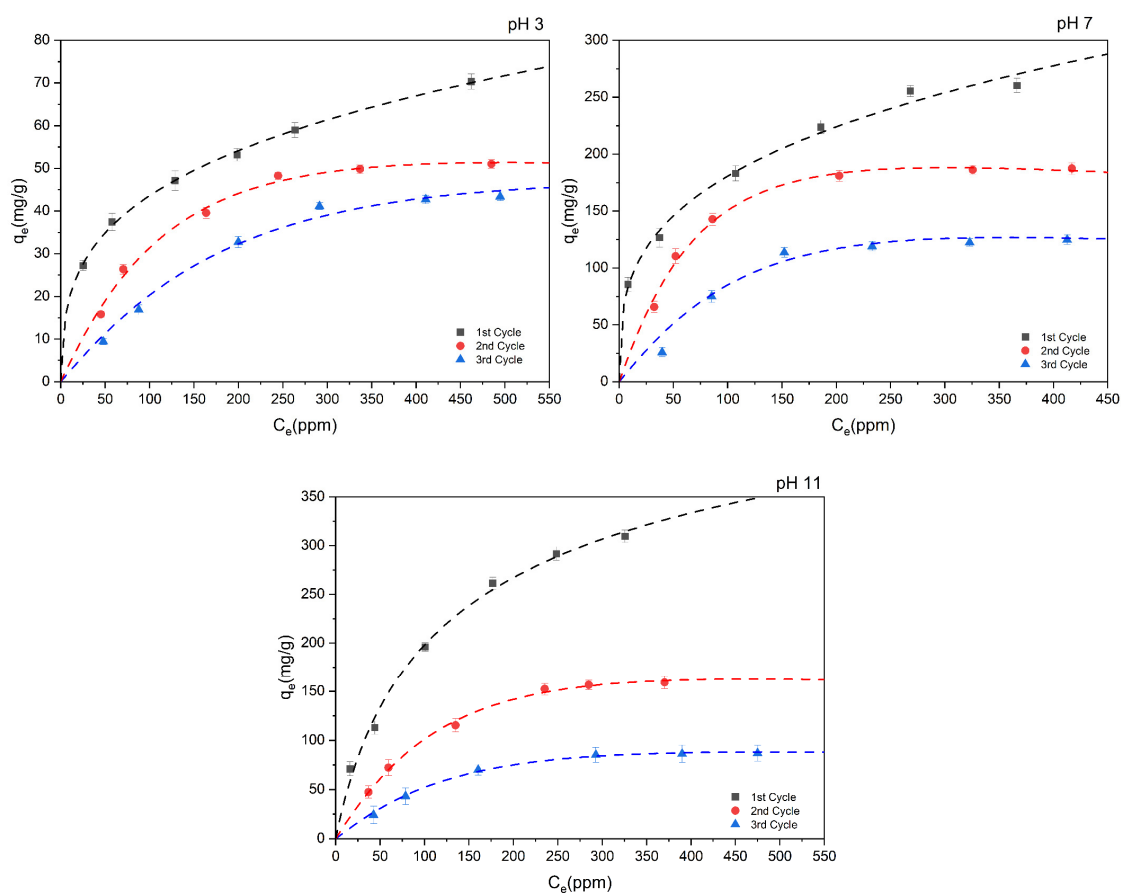
Figure 13. Evaluation of the adsorption capacity of metformin in R:F-0.40 with several cycles reusing, variation in the initial concentration of metformin from 50 to 500 mg/L at pH 7, 25 °C for 7 days.

4. Conclusions

The study on metformin adsorption onto R:F xerogels presented a comprehensive exploration of crucial factors influencing adsorption processes, with implications for water purification and environmental sustainability. The xerogel synthesis process yields

interconnected polyaromatic structures, creating differences between acidic and basic sites on the xerogel structure, which were essential for adsorption characteristics. Extensive physicochemical characterization highlighted structural modification's impact on adsorption capacity, showcasing the tunability of xerogel properties. Furthermore, FT-IR analysis revealed crucial transformations during polymerization, while variation in acidic and basic sites influences adsorption selectivity. Moreover, XRD showed an amorphous nature and smaller particle sizes with increasing R:F ratios. In addition, the SEM and TEM indicated high R:F ratios, resulting in large particle sizes and improved crystallinity, which correlate with high carbon content. Additionally, adsorption equilibrium studies demonstrated increased adsorption capacity at higher metformin concentrations, emphasizing the xerogel's impressive adsorption capacity of 325 mg/g, surpassing the previous literature (Table 2). pH plays a significant role, with low pH decreasing adsorption due to electrostatic attractions, while higher pH enhances adsorption through electrostatic attractions and hydrogen bonding. On the other hand, thermodynamic analysis revealed that endothermic adsorption was favored at high temperatures, underscoring the importance of temperature control. Also, negative values of ΔG^0 involved spontaneous adsorption, driven by favorable interactions such as hydrogen bonds or electrostatic forces. These findings contribute to our understanding of metformin adsorption onto R:F xerogels and have significant practical implications. Additionally, the competitive behavior of Na^+, Mg^{2+}, and Ca^{2+} ions for active sites induces ion exchange and influences adsorption capacity. Finally, computational simulations and experimental results confirmed that high pH values favor metformin adsorption, while urea and creatinine in simulated urine decrease adsorption capacity, affecting adsorbent selectivity. Further, reuse cycle evaluations highlighted pH 7 as optimal for maintaining competitive adsorption capacity, showing an immobilization of metformin for the xerogel due to strong interactions. Moreover, these practical implications were crucial for designing efficient adsorbent systems for contaminant removal in water treatment and pharmaceutical purification processes, addressing critical environmental protection and resource efficiency challenges.

Supplementary Materials: The following supporting information can be downloaded at: https://www.mdpi.com/article/10.3390/pr12071431/s1, Figure S1: Speciation diagram of metformin, Figure S2: Optimized structure of metformin for different pH values: neutral and negative modes, Figure S3: Polymerization mechanism of xerogels, Figure S4: Concentration of acidic and basic active sites of xerogels R:F-0.05 to F:R-0.40, Figure S5: Patterns X-ray diffraction of xerogels synthesized, Figure S6: FT-IR spectra of the adsorption of metformin in R:F-0.40, varying the initial concentration of metformin from 100 to 500 mg/L (pH 7 and 25 °C), Figure S7: SEM micrographs and element mapping analysis for particle analysis from the metformin adsorption process result in R:F-0.40, Figure S8: Thermal gravimetric analysis of metformin, R:F-0.40, and RF:0.40 with metformin, Figure S9: Optimized structure of adsorption modes of metformin for three pH values in the gas phase., Figure S10: FT-IR spectra of the adsorption of metformin, metformin–urea andS1 metformin–urea–creatine in R:F-0.40, at 50 mg/L, pH 7, and 25 °C, Figure S11: Scheme of electron surface for the interaction of the R:F-0.40 monomer with metformin, urea, and creatine., Figure S12: UV–vis spectrum of synthetic urine, synthetic urine with metformin (50 mg/L) before and after the adsorption process with R:F-0.40, at pH 7, 25 °C, for 7 days, Figure S13: Analysis of the adsorption capacity of metformin absorbed by R:F-0.40 after three use cycles, Figure S14: FT-IR spectra of original R:F-0.40 and after three cycles of refusal in the adsorption of metformin at pH 3, 7, and 11, at 50 mg/L, pH 7, and 25 °C; Table S1: Analysis of the adjustment of the experimental metformin adsorption isotherms at R:F-0.05 to 0.40, using the Langmuir, Freundlich, and Prausnitz–Radke models, Table S2: Adsorption energies (Eads) of adsorption modes of metformin for three pH values in the gas phase, Table S3: Adsorption energies (Eads) of adsorption modes of metformin for three pH values in gas and aqueous phases, Table S4: Cartesian coordinates of the different geometries for metformin–xerogel complex on gas phase, Table S5: Cartesian coordinates of the different geometries for metformin–xerogel complex on aqueous solution. Reference [41] is cited in the supplementary materials.

References

1. Foretz, M.; Guigas, B.; Bertrand, L.; Pollak, M.; Viollet, B. Metformin: From Mechanisms of Action to Therapies. *Cell Metab.* **2014**, *20*, 953–966. [CrossRef]
2. Hernández, B.; Pflüger, F.; Kruglik, S.G.; Cohen, R.; Ghomi, M. Protonation–deprotonation and structural dynamics of antidiabetic drug metformin. *J. Pharm. Biomed. Anal.* **2015**, *114*, 42–48. [CrossRef]
3. Balakrishnan, A.; Sillanpää, M.; Jacob, M.M.; Vo, D.-V.N. Metformin as an emerging concern in wastewater: Occurrence, analysis and treatment methods. *Environ. Res.* **2022**, *213*, 113613. [CrossRef]
4. Desai, D.; Wong, B.; Huang, Y.; Ye, Q.; Tang, D.; Guo, H.; Huang, M.; Timmins, P. Surfactant-Mediated Dissolution of Metformin Hydrochloride Tablets: Wetting Effects Versus Ion Pairs Diffusivity. *J. Pharm. Sci.* **2014**, *103*, 920–926. [CrossRef]
5. Boehm, H.P.; Diehl, E.; Heck, W.; Sappok, R. Surface Oxides of Carbon. *Angew. Chem. Int. Ed. Engl.* **1964**, *3*, 669–677. [CrossRef]
6. Ramírez-Muñiz, K.; Song, S.; Berber-Mendoza, S.; Tong, S. Adsorption of the complex ion Au(CN)2- onto sulfur-impregnated activated carbon in aqueous solutions. *J. Colloid Interface Sci.* **2010**, *349*, 602–606. [CrossRef]
7. Sarigul, N.; Korkmaz, F.; Kurultak, İ. A New Artificial Urine Protocol to Better Imitate Human Urine. *Sci. Rep.* **2019**, *9*, 20159. [CrossRef]
8. Ocampo-Pérez, R.; Leyva-Ramos, R.; Sanchez-Polo, M.; Rivera-Utrilla, J. Role of pore volume and surface diffusion in the adsorption of aromatic compounds on activated carbon. *Adsorption* **2013**, *19*, 945–957. [CrossRef]
9. Frisch, M.J.; Hiscocks, J. *Gaussian 09*; Gaussian, Inc.: Pittsburgh, PA, USA, 2009.
10. Al-Muhtaseb, S.A.; Ritter, J.A. Preparation and Properties of Resorcinol–Formaldehyde Organic and Carbon Gels. *Adv. Mater.* **2003**, *15*, 101–114. [CrossRef]
11. Pekala, R.W. Organic aerogels from the polycondensation of resorcinol with formaldehyde. *J. Mater. Sci.* **1989**, *24*, 3221–3227. [CrossRef]
12. Heidari, B.S.; Cheraghchi, V.-S.; Motahari, S.; Motlagh, G.H.; Davachi, S.M. Optimized mercapto-modified resorcinol formalde-hyde xerogel for adsorption of lead and copper ions from aqueous solutions. *J. Sol-Gel Sci. Technol.* **2018**, *88*, 236–248. [CrossRef]
13. Khamkure, S.; Gamero-Melo, P.; Garrido-Hoyos, S.E.; Reyes-Rosas, A.; Pacheco-Catalán, D.-E.; López-Martínez, A.M. The Development of Fe_3O_4-Monolithic Resorcinol-Formaldehyde Carbon Xerogels Using Ultrasonic-Assisted Synthesis for Arsenic Removal of Drinking Water. *Gels* **2023**, *9*, 618. [CrossRef]
14. Ficanha, A.M.M.; Oro, C.E.D.; Franceschi, E.; Dallago, R.M.; Mignoni, M.L. Evaluation of Different Ionic Liquids as Additives in the Immobilization of Lipase CAL B by Sol-Gel Technique. *Appl. Biochem. Biotechnol.* **2021**, *193*, 2162–2181. [CrossRef]
15. Gaikwad, M.M.; Kakunuri, M.; Sharma, C.S. Enhanced catalytic graphitization of resorcinol formaldehyde derived carbon xerogel to improve its anodic performance for lithium ion battery. *Mater. Today Commun.* **2019**, *20*, 100569. [CrossRef]
16. AlAreeqi, S.; Bahamon, D.; Polychronopoulou, K.; Vega, L.F. Insights into the thermal stability and conversion of carbon-based materials by using ReaxFF reactive force field: Recent advances and future directions. *Carbon* **2022**, *196*, 840–866. [CrossRef]
17. Sundqvist, B. Carbon under pressure. *Phys. Rep.* **2021**, *909*, 1–73. [CrossRef]
18. Bystrzejewski, M.; Lange, H.; Huczko, A.; Elim, H.; Ji, W. Study of the optical limiting properties of carbon-encapsulated magnetic nanoparticles. *Chem. Phys. Lett.* **2007**, *444*, 113–117. [CrossRef]
19. Gorman, M. The evidence from infrared spectroscopy for hydrogen bonding: A case history of the correlation and interpretation of data. *J. Chem. Educ.* **1957**, *34*, 304. [CrossRef]
20. Long, D.A. Infrared and Raman characteristic group frequencies. Tables and charts George Socrates John Wiley and Sons, Ltd, Chichester, Third Edition, 2001. Price pound sterling 135. *J. Raman Spectrosc.* **2004**, *35*, 905. [CrossRef]

21. Comí, M.; Fernández, M.; Santamaría, A.; Lligadas, G.; Ronda, J.C.; Galià, M.; Cádiz, V. Carboxylic Acid Ionic Modification of Castor-Oil-Based Polyurethanes Bearing Amine Groups: Chemically Tunable Physical Properties and Recyclability. *Macromol. Chem. Phys.* **2017**, *218*, 1700379. [CrossRef]

22. Zhu, S.; Liu, Y.-G.; Liu, S.-B.; Zeng, G.-M.; Jiang, L.-H.; Tan, X.F.; Zhou, L.; Zeng, W.; Li, T.-T.; Yang, C.-P. Adsorption of emerging contaminant metformin using graphene oxide. *Chemosphere* **2017**, *179*, 20–28. [CrossRef]

23. Balasubramani, K.; Sivarajasekar, N.; Naushad, M. Effective adsorption of antidiabetic pharmaceutical (metformin) from aqueous medium using graphene oxide nanoparticles: Equilibrium and statistical modelling. *J. Mol. Liq.* **2020**, *301*, 112426. [CrossRef]

24. Kyzas, G.Z.; Nanaki, S.G.; Koltsakidou, A.; Papageorgiou, M.; Kechagia, M.; Bikiaris, D.N.; Lambropoulou, D.A. Effectively designed molecularly imprinted polymers for selective isolation of the antidiabetic drug metformin and its transformation product guanylurea from aqueous media. *Anal. Chim. Acta* **2015**, *866*, 27–40. [CrossRef]

25. Spessato, L.; Duarte, V.A.; Viero, P.; Zanella, H.; Fonseca, J.M.; Arroyo, P.A.; Almeida, V.C. Optimization of Sibipiruna activated carbon preparation by simplex-centroid mixture design for simultaneous adsorption of rhodamine B and metformin. *J. Hazard. Mater.* **2021**, *411*, 125166. [CrossRef]

26. Sanchez-Silva, J.M.; Collins-Martínez, V.H.; Padilla-Ortega, E.; Aguilar-Aguilar, A.; Labrada-Delgado, G.J.; Gonzalez-Ortega, O.; Palestino-Escobedo, G.; Ocampo-Pérez, R. Characterization and transformation of nanche stone (*Byrsonima crassifolia*) in an activated hydrochar with high adsorption capacity towards metformin in aqueous solution. *Chem. Eng. Res. Des.* **2022**, *183*, 580–594. [CrossRef]

27. Dave, P.N.; Kamaliya, B.; Macwan, P.M.; Trivedi, J.H. Fabrication and characterization of a gum ghatti-cl-poly(N-isopropyl acrylamide-co-acrylic acid)/CoFe2O4 nanocomposite hydrogel for metformin hydrochloride drug removal from aqueous solution. *Curr. Res. Green Sustain. Chem.* **2023**, *6*, 100349. [CrossRef]

28. Szalewicz, K. *Hydrogen Bond, in Encyclopedia of Physical Science and Technology*, 3rd ed.; Meyers, R.A., Ed.; Academic Press: New York, NY, USA, 2003; pp. 505–538.

29. Fu, L.; Li, J.; Wang, G.; Luan, Y.; Dai, W. Adsorption behavior of organic pollutants on microplastics. *Ecotoxicol. Environ. Saf.* **2021**, *217*, 112207. [CrossRef]

30. Badran, I.; Hassan, A.; Manasrah, A.D.; Nassar, N.N. Experimental and theoretical studies on the thermal decomposition of metformin. *J. Therm. Anal. Calorim.* **2019**, *138*, 433–441. [CrossRef]

31. Adnan; Omer, M.; Khan, B.; Khan, I.; Alamzeb, M.; Zada, F.M.; Ullah, I.; Shah, R.; Alqarni, M.; Simal-Gandara, J. Equilibrium, Kinetic and Thermodynamic Studies for the Adsorption of Metanil Yellow Using Carbonized Pistachio Shell-Magnetic Nanoparticles. *Water* **2022**, *14*, 4139. [CrossRef]

32. Aljamali, N.; Khdur, R.; Alfatlawi, I. Physical and Chemical Adsorption and its Applications. *Int. J. Thermodyn. Chem. Kinet.* **2021**, *7*, 1–8.

33. De Gisi, S.; Lofrano, G.; Grassi, M.; Notarnicola, M. Characteristics and adsorption capacities of low-cost sorbents for wastewater treatment: A review. *Sustain. Mater. Technol.* **2016**, *9*, 10–40. [CrossRef]

34. Kłonkowski, A.M.; Grobelna, B.; Widernik, T.; Jankowska-Frydel, A.; Mozgawa, W. The Coordination State of Copper(II) Complexes Anchored and Grafted onto the Surface of Organically Modified Silicates. *Langmuir* **1999**, *15*, 5814–5819. [CrossRef]

35. Torres, C.E.I.; Quezada, T.E.S.; Kharissova, O.V.; Kharisov, B.I.; de la Fuente, M.I.G. Carbon-based aerogels and xerogels: Synthesis, properties, oil sorption capacities, and DFT simulations. *J. Environ. Chem. Eng.* **2021**, *9*, 104886. [CrossRef]

36. Sun, A.; Hou, X.; Hu, X. Super-performance photothermal conversion of 3D macrostructure graphene-CuFeSe2 aerogel contributes to durable and fast clean-up of highly viscous crude oil in seawater. *Nano Energy* **2020**, *70*, 104511. [CrossRef]

37. Zou, C.-Y.; Ji, W.; Shen, Z.; Tang, Q.; Fan, M. NH3 molecule adsorption on spinel-type ZnFe2O4 surface: A DFT and experimental comparison study. *Appl. Surf. Sci.* **2018**, *442*, 778–786. [CrossRef]

38. Serna-Carrizales, J.C.; Zárate-Guzmán, A.I.; Aguilar-Aguilar, A.; Forgionny, A.; Bailón-García, E.; Flórez, E.; Gómez-Durán, C.F.A.; Ocampo-Pérez, R. Optimization of Binary Adsorption of Metronidazole and Sulfamethoxazole in Aqueous Solution Supported with DFT Calculations. *Processes* **2023**, *11*, 1009. [CrossRef]

39. Forgionny, A.; Acelas, N.Y.; Jimenez-Orozco, C.; Flórez, E. Toward the design of efficient adsorbents for Hg^{2+} removal: Molecular and thermodynamic insights. *Int. J. Quantum Chem.* **2020**, *120*, e26258. [CrossRef]

40. Rubtsov, I.V.; Kumar, K.; Hochstrasser, R.M. Dual-frequency 2D IR photon echo of a hydrogen bond. *Chem. Phys. Lett.* **2005**, *402*, 439–443. [CrossRef]

41. Kafle, B.P. Chapter 6—Introduction to nanomaterials and application of UV–Visible spectroscopy for their characterization. In *Chemical Analysis and Material Characterization by Spectrophotometry*; Kafle, B.P., Ed.; Elsevier: Amsterdam, The Netherlands, 2020; pp. 147–198.